

Neutrino oscillation physics at an upgraded CNGS with large next generation liquid Argon TPC detectors

A. Meregaglia¹ and A. Rubbia²

Institut für Teilchenphysik, ETHZ, CH-8093 Zürich, Switzerland

Abstract

The determination of the missing U_{e3} element (magnitude and phase) of the PMNS neutrino mixing matrix is possible via the detection of $\nu_\mu \rightarrow \nu_e$ oscillations at a baseline L and energy E given by the atmospheric observations, corresponding to a mass squared difference $E/L \sim \Delta m^2 \simeq 2.5 \times 10^{-3} \text{ eV}^2$. While the current optimization of the CNGS beam provides limited sensitivity to this reaction, we discuss in this document the physics potential of an intensity upgraded and energy re-optimized CNGS neutrino beam coupled to an off-axis detector. We show that improvements in sensitivity to θ_{13} compared to that of T2K and NoVA are possible with a next generation large liquid Argon TPC detector located at an off-axis position (position rather distant from LNGS, possibly at shallow depth). We also address the possibility to discover CP-violation and disentangle the mass hierarchy via matter effects. The considered intensity enhancement of the CERN SPS has strong synergies with the upgrade/replacement of the elements of its injector chain (Linac, PSB, PS) and the refurbishing of its own elements, envisioned for an optimal and/or upgraded LHC luminosity programme.

Keywords: neutrino experiments, neutrino oscillations, CP-violation, liquid argon, TPC

1 Introduction

The new CERN CNGS neutrino beam [1], directed towards Italy, has recently begun operation. First events have been collected in the OPERA detector [2] at LNGS [3]. The goal of this first phase is to unambiguously detect the appearance of τ leptons induced by ν_τ CC events, thereby proving the $\nu_\mu \rightarrow \nu_\tau$ flavor oscillation.

The OPERA result, together with well established observations of solar and atmospheric neutrinos, in particular from Superkamiokande [4], SNO [5] and KamLAND [6], will most likely confirm the validity of the 3×3 PMNS [7] mixing matrix approach to describe all the observed neutrino flavor conversion phenomena.

However, in order to complete this picture, all the elements (magnitude and phase) of the mixing matrix must be determined. That includes the U_{e3} element for which today there is only an upper bound corresponding in the standard parameterization to $\sin^2 2\theta_{13} \lesssim 0.1$ (90%C.L.) from the CHOOZ [8] reactor experiment.

The determination of this missing element is possible via the detection of $\nu_\mu \rightarrow \nu_e$ oscillations at a baseline L and energy E given by the atmospheric observations, corresponding to a

¹anselmo.meregaglia@cern.ch

²andre.rubbia@cern.ch

mass squared difference $E/L \sim \Delta m^2 \simeq 2.5 \times 10^{-3} \text{ eV}^2$. The current optimization of the CNGS beam provides limited sensitivity to this reaction and OPERA should reach a sensitivity $\sin^2 2\theta_{13} \lesssim 0.06$ (90%C.L.) in 5 years of running. ICARUS T600 [9, 10, 11, 12, 13], to be commissioned in the coming years, will detect too few contained CNGS events to competitively study electron appearance. The T2K [14] and NoVA [15] accelerator projects are on the other hand optimized for searching for electron appearance and should reach a sensitivity $\sin^2 2\theta_{13} \lesssim 0.01$ (90%C.L.) some time after 2010. DOUBLE-CHOOZ [16] will also attempt to detect a small $\nu_e \rightarrow \nu_x$ disappearance effect from reactors, aiming for a result before the two previous projects at accelerators.

A non vanishing $|U_{e3}|$ would open the possibility of CP/T violation in the leptonic sector, as a direct consequence of non-trivial complex phases in the 3×3 mixing matrix. In the case of neutrino flavor oscillations, there is only one relevant phase in the mixing matrix, called δ_{CP} . The condition $\delta_{\text{CP}} \neq 0$ would induce different flavor transition probabilities for neutrinos and antineutrinos. The observation of this effect is one of the main challenges of future neutrino oscillation experiments. On the other hand, due to matter effects, neutrinos and antineutrinos propagate differently through the Earth. This will also induce differences in oscillatory behaviors of neutrinos and antineutrinos that are rather small at the baseline considered here, however will affect the sensitivity of an unambiguous determination of the value of the mixing matrix complex phase.

In this document we discuss the physics potential beyond the approved OPERA programme, of an intensity upgraded and energy re-optimized CNGS neutrino beam coupled to new off-axis detectors, and show that improvements in sensitivity to θ_{13} compared to that of T2K and NoVA are possible with a next generation large liquid Argon TPC detector located at an appropriately chosen off-axis position. As location, a “green-field site”, rather distant from LNGS, presumably at shallow depth is envisaged [17]. In the green-field site, a dedicated shaft would be dug in the ground with a depth of about 200 m and a cavern capable of hosting the detector would be excavated at this depth. With such a facility, the possibility to discover CP-violation and disentangle the mass hierarchy via matter effects is also addressed.

The considered intensity enhancement of the CERN SPS has strong synergies with the upgrade/replacement of the elements of its injector chain (Linac, PSB, PS) and the refurbishing of its own elements, envisioned for an optimal and/or upgraded LHC luminosity programme.

2 Possible upgrades of the CNGS beam

2.1 A comparison with other facilities

The CNGS is a “conventional” neutrino beam, in which most neutrinos are produced by the decay of secondary pions/kaons obtained in high-energy collisions of protons on an appropriate target and followed by a magnetic focusing system. In this kind of beams, the neutrino spectrum and the flux are essentially determined by four parameters:

- the primary proton energy E_p impinging on the target,
- the number of protons on target N_{pot} per year,
- the focusing system, which focuses a fraction of the secondary charged pions and kaons (positive, negative or both signs depending on the focusing device),
- the angle θ_ν between the parent meson flight direction and the direction of the detector at the far distance.

	JPARC		FNAL		CERN		
	design	upgrade	w/o PD	w PD	CNGS dedicated	CNGS'	CNGS+
Proton energy E_p	40 GeV/c		120 GeV/c		400 GeV/c		
$ppp(\times 10^{13})$	33	> 33	9.5	15	4.8	7	14
T_c (s)	3.64	< 3.64	1.6	1.467	6	6	6
Efficiency	1.0	1.0	1.0	1.0	0.55	0.55	0.83
Running (d/y)	130	130	230	230	200	200	200
$N_{pot} / \text{yr} (\times 10^{19})$	100	$\simeq 700$	120	200	7.6	11	33
Beam power (MW)	0.6	4	1.1	2.0	0.3	0.4	1.2
$E_p \times N_{pot}$ ($\times 10^{22}$ GeV \times pot/yr)	4	28	14.4	24	3	4.4	13.2

Table 1: Assumed parameters for the various beams at JPARC [18] , FNAL [21, 20] and CERN [1, 24, 25].

The current nominal proton intensity per CNGS pulse is 4.8×10^{13} at 400 GeV/c¹. This number is only slightly below the intensity record achieved in the SPS in 1997 after careful tuning of all the accelerator complex. Since that time the CERN PS and SPS machines have had major upgrades in preparation for the LHC beam. In September 2004 a total intensity of 5.3×10^{13} was accelerated to top energy in the SPS. Following the studies for the CNGS, it was found that the RF acceleration of the SPS could be shortened by 0.2 s, allowing to reduce the length of the CNGS cycle from 6.2 s to 6.0 s, with a considerable positive impact for the possible protons on the CNGS target, since the total cycle could be reduced from 7.2 s to 6.0 s.

In dedicated mode, the CNGS should be able to deliver 7.6×10^{19} pots/year [1]. This is computed assuming 4.8×10^{13} ppp , a cycle of 6 seconds, a running of 200 days and an efficiency of 55%, corresponding to a beam power of 0.3 MW. This is summarized in Table 1. This situation is to be contrasted with the JPARC or FNAL facilities.

At JPARC the baseline power is 0.75 MW [18]. Using a design 33×10^{13} ppp , a cycle of 3.64 seconds, a running of 130 days and an efficiency of 100% at 40 GeV/c actually yields a beam power of 0.6 MW. Starting in 2009, the beam power should be 0.1 MW and be ramped up to design intensity and beyond in the following years [19]. Future upgrades of the JPARC complex consider an increase of protons per pulse and a reduced cycling time, to bring up the power to 4 MW, although this is known to be a rather challenging goal.

At FNAL the current design of the NUMI facility should be 400 kW. From May 2005 until March 2006, an average of 165 kW with a peak at 270 kW has been achieved [20]. After the FNAL collider shuts down, better performances should be reachable at the NUMI beam. With 9.5×10^{13} ppp , a fast cycle of 1.6 seconds, a running of 230 days at an efficiency of 100% with an energy of 120 GeV/c, a beam power of 1.1 MW is attained. A completely new proton driver (a 8 GeV linac) could raise the power to 2 MW [21]. Plans to reach similar beam powers exist at BNL [22].

¹We recall that the aperture of the extraction line from the SPS to the CNGS target is designed for protons with momenta above 350 GeV/c.

2.2 An upgraded CNGS at the CERN SPS ?

In fact, a relevant figure to compare neutrino yields is the product of the energy of the protons E_p times the integrated number of protons on target N_{pot} . This product per year is listed in the last row of Table 1. For JPARC, the product will be 4×10^{22} GeV \times pot/yr increasing to 28×10^{22} GeV \times pot/yr for a 4 MW beam. At FNAL, after the collider shuts down, the integrated intensity should reach 14.4×10^{22} GeV \times pot/yr with a possibility to double this value with a completely new proton driver. At CERN dedicated CNGS, the number is 3×10^{22} GeV \times pot/yr, similar to that of JPARC for 1 MW beam power. Can one increase the intensity of CNGS to reach an integrated product of $\mathcal{O}(10^{23})$ GeV \times pot/yr ?

The main focus of the CERN accelerator complex will soon shift to LHC. However, it is known that the integrated luminosity in the LHC experiments will directly depend upon the performance and reliability of the injectors, namely Linac2, PSB, PS and SPS. The CERN working group on Proton Accelerators for the Future (PAF) has reviewed the situation and elaborated a baseline scenario for the upgrades of the CERN accelerators [24]. In the first stage, a new Linac4 would be built to simplify the operation of the PS complex for LHC and help investigate the SPS capability to handle very high brightness beams. In a second stage, the PS would be replaced by a new PS (PS+) with a beam power of approximately 200 kW available at 50 GeV/c [25]. If the proton beam from the new PS could be efficiently post-accelerated to 400 GeV/c and extracted to the CNGS target area, a MW-class neutrino beam would be possible.

As specific example (to be further studied), a re-optimized PS+SPS complex could aim at reaching 7×10^{13} *ppp* (we recall that the current record is 5.3×10^{13} protons accumulated in the SPS) which corresponds to the design maximum pulse of the current CNGS target. With the new injection at 50 GeV/c provided by a new PS, about twice as many protons should be potentially accumulated in the SPS as compared to today's situation. Since in addition the reliability of the complex should be increased with a new PS+ replacing the $\simeq 40$ years old PS, one can assume that the efficiency will become 0.83 instead of the currently assumed 0.55. Hence, with the increase of a factor ≈ 2.5 of the proton-per-pulse intensity and a slight improvement in the efficiency could bring the CNGS power to 1.2 MW.

3 Next generation detectors

When searching for ν_e appearance there will be both an irreducible intrinsic ν_e background and a background due to event misidentification. In a next generation experiment one should aim at reducing the backgrounds from event misidentification as much as possible in order to profit at most from the increased statistics. Eventually, the limiting factor will be the knowledge of the intrinsic ν_e background so other sources of backgrounds should be suppressed below this contamination, which is generally at the level of the percent in the region of the oscillation maximum. This is not the case in T2K and NoVA where a ratio $\nu_e : NC \pi^0 \simeq 1 : 1$ is achieved at the cost of efficiency ($\epsilon \approx 40\%$ for T2K, $\approx 20\%$ for NoVA).

We note that thanks to the progress in predicting neutrino fluxes and cross-sections given the extended campaigns of hadro-production measurements and the running of, or plans for, dedicated neutrino cross-section-measurement experiments (see Refs. [26, 27] for a recent review), we can expect that the systematic error on the prediction of the intrinsic ν_e background (\equiv the number of background events) will be below 5%². Hence, the error on the contamination,

²In the NOMAD experiment, a prediction of the ν_e contamination with relative systematic errors between energy bins varying between 4 and 7% was shown to be possible with the retuning of the hadron production

effectively limiting the sensitivity to electron appearance, is at the level of $\lesssim 0.01 \times 0.05 \simeq 5 \times 10^{-4}$. Hence, if statistic permits, new generation detectors at conventional superbeams should allow to probe oscillation signals at the per-mil level before they become dominated by this systematic error.

The liquid Argon Time Projection Chamber (LAr TPC) [9, 10, 11, 12, 13] is a powerful detector for uniform and high accuracy imaging of massive active volumes. It is based on the fact that in highly pure Argon, ionization tracks can be drifted over distances of the order of meters. Imaging is provided by position-segmented electrodes at the end of the drift path, continuously recording the signals induced. T_0 is provided by the prompt scintillation light.

Our analysis assumes the concept of a liquid Argon TPC with mass order of 100 kton, as proposed in [29]. Other designs have been presented in Ref. [30]. An LOI based on a more standard configuration and a surface detector has also been submitted to FNAL [31]. A document describing physics with next generation liquid Argon detectors was submitted as a memorandum to the CERN SPSC for the Villars workshop in April 2004 [32].

The design of Ref. [29] relies on (a) industrial tankers developed by the petrochemical industry (no R&D required, readily available, safe) and their extrapolation to underground or shallow depth LAr storage, (b) novel readout method for very long drift paths with e.g. LEM readout, (c) new solutions for very high drift voltage, (d) a modularity at the level of 100 kton (limited by cavern size) and (e) the possibility to embed the LAr in a magnetic field [33, 34, 35]. Such a scalable, single LAr tanker design is the most attractive solution from the point of view of physics, detector construction, operation and cryogenics, and finally cost. An R&D program is underway with the aim of optimizing the design [36]. This is also consistent with the recommendations of the SPSC at Villars.

The liquid Argon TPC imaging offers optimal conditions to reconstruct with very high efficiency the electron appearance signal in the energy region of interest in the GeV range, while considerably suppressing the NC background consisting of misidentified π^0 's. MC studies show that an efficiency above 90% for signal can be achieved while suppressing NC background to the permil level [37]. This MC result was shown to be true over a wide range of neutrino energy, typ. between 0 and 5 GeV. If verified experimentally, this implies that the intrinsic ν_e background will be the dominant background in superbeams coupled to liquid Argon TPCs. For this purpose, a test-beam dedicated to the reconstruction and separation of electrons from neutral pions has been discussed [38]. A $\simeq 100$ ton liquid Argon TPC to complement the 1 kton Water Cerenkov detector at the potential 2 km site 2.5° off-axis from the T2K beam has also been proposed [37]. If realized, this unique experimental setup will allow to compare the performance of the liquid Argon TPC to the Water Cerenkov ring imaging and to reconstruct neutrino events directly in the same beam.

4 Proposed beam optics and expected event rates

The CNGS decay tunnel is directed towards south-east in the direction of the LNGS laboratory in Italy. The profile of the resulting neutrino beam is displayed in Figure 1. While the distance from CERN to the LNGS for neutrino oscillations is 732 km, baselines from 500 to 1100 km at various angles can be readily envisaged in the off-axis configuration, given the advantageous geographic alignment of the Italian peninsula. Since for a baseline of that order the first maximum of the oscillation will occur at an energy $\simeq 2$ GeV, the neutrino beam must be optimized to relatively low-energy.

model and a precise simulation of the geometry of the beam line, in particular the target region [28].

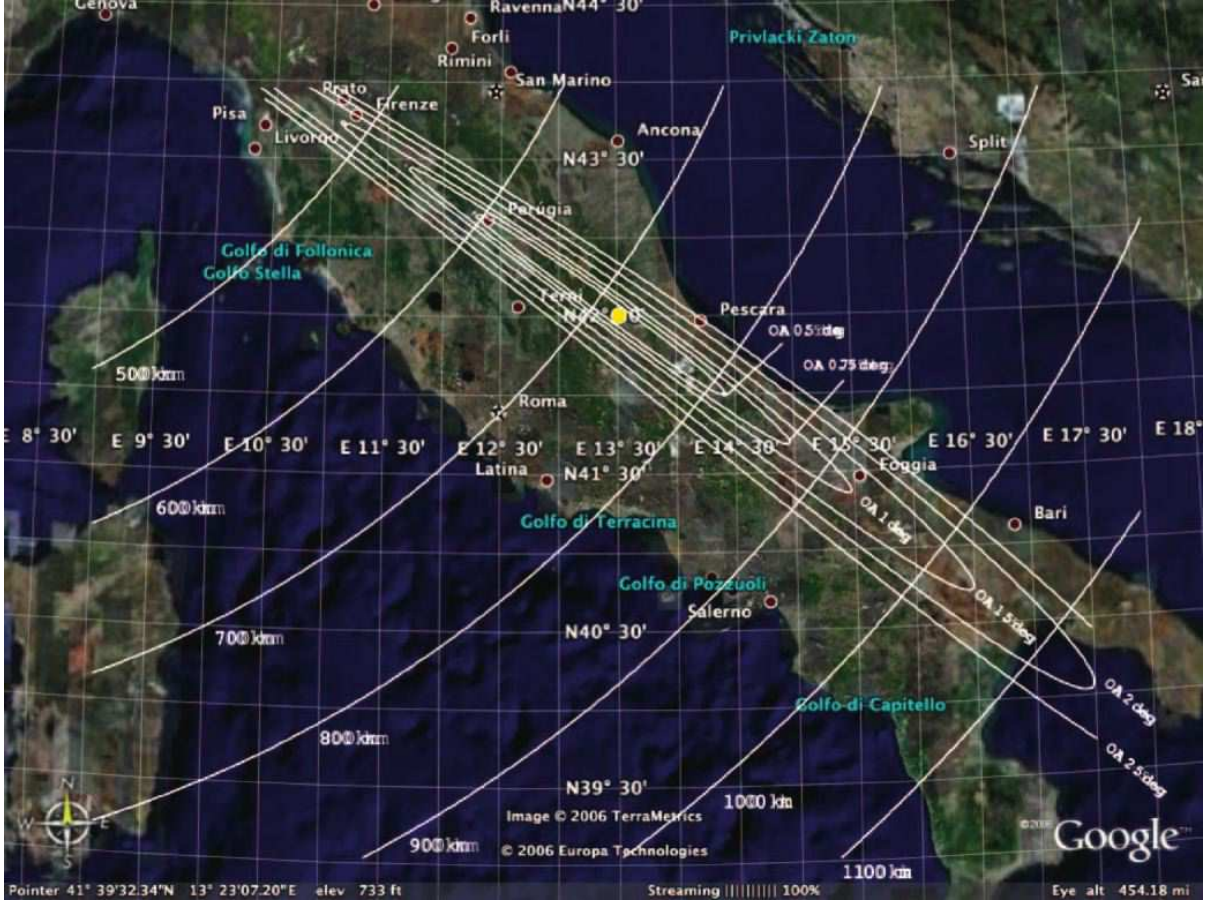


Figure 1: Italy map and beam contours for OA0.5, OA0.75, OA1, OA1.5, OA2 and OA2.5 degrees. The corresponding baselines from CERN are also shown (from 500 to 1100 km).

The present CNGS design [1] is optimized for ν_τ appearance (in what follows referred to as “CNGS τ ”), thus for a relatively high-energy neutrino beam. As already mentioned, the 400 GeV/c SPS beam will nominally deliver 4.5×10^{19} protons per year on a graphite target, made of spaced thin rods to reduce the re-interaction rate within the target. The two magnetic horns (horn and reflector) are tuned to focus 35 and 50 GeV/c mesons, with an acceptance of the order of 30 mrad.

4.1 The CNGS low energy (L.E.) on-axis option

In Ref. [39], some of us have studied an optimization of the CNGS optics (in what follows referred to as “CNGS L.E.”) that would allow to increase the neutrino flux yield at low energy by a factor 5 compared to the baseline τ -optimization of the CNGS beam. To improve particle yield at low energies, the focusing system was re-designed, the target dimensions were changed and the effective decay tunnel length was shortened. The main differences with the present (τ) design are summarized in Table 2.

The neutrino energy of interest corresponded to pions in the range 0.7-5.5 GeV. To focus these pions, a standard double-horn system was adopted. Both magnetic devices had to be placed near to or even around the target, to capture particles emitted at relatively large angles. The present CNGS shielding and collimator openings would not allow more than 100 mrad. The

	CNGS τ	CNGS L.E.	CNGS 10 GeV
Target			
Material	Carbon	Carbon	Carbon
Total target length	2 m	1 m	2 m
Number of rods	13	1	8
Rod spacing	first 8 with 9 cm dist.	none	9 cm
Diameter of rods	first 2 5 mm, then 4 mm	4mm	2 mm
Horn			
Distance beginning of target-horn entrance	320 cm	25 cm	100 cm
Length	6.65 m	4 m	6.65 m
Outer conductor radius	35.8 cm	80 cm	37.2 cm
Inner conductor max. radius	6.71 cm	11.06 cm	11.4 cm
Inner conductor min. radius	1.2 cm	0.2 cm	0.15 cm
Current	150kA	300kA	140kA
Reflector			
Distance beginning of target-reflector entrance	43.4 m	6.25 m	11 m
Length	6.65 m	4 m	6.45 m
Outer conductor radius	55.8 cm	90 cm	56.6 cm
Inner conductor max. radius	28 cm	23.6 cm	24 cm
Inner conductor min. radius	7cm	5 cm	6 cm
Current	180kA	150kA	180kA
Decay tunnel			
Distance beginning of target-tunnel entrance	100 m	50 m	100 m
Length	992 m	350 m	1100 m*
Radius	122 cm	350 cm	122 cm

Table 2: Parameter list for the present CNGS design and the “new” beams for low energy ν 's. The parameters for the CNGS 10 GeV configuration can probably still be optimized. (*) actual length of decay tunnel does not play a role for CNGS 10 GeV configuration.

secondary particles had to be bent before they travelled too far away in radius, therefore the horn magnetic field had to be high enough. This also meant that the horn was shorter than the ones used to focus high energy beams, because the particles should not have travelled in the magnetic field for a distance longer than their curvature radius.

We obtained good focusing capability with two four meters long horns. The horn current had been set at 300kA, the reflector one at 150kA. The horn started 25 cm after the target entrance face, the reflector started just two meters after the horn end. Horn and reflector shapes had been computed to focus 2 GeV/c and 3 GeV/c particles respectively. We were aware that these (parabolic) horn shapes were derived in the approximation of point-like source. However, detailed Monte Carlo calculations verified the good focusing capabilities of the system. The focusing efficiency in the range of interest was around 50%.

The resulting CNGS L.E. beam is shown in Figure 2. As mentioned, in comparison to the CNGS τ beam, the rate around 2 GeV is increased by about a factor 5.

4.2 The CNGS off-axis options

4.2.1 The off-axis technique

The “off-axis” technique, pioneered in the Brookhaven neutrino oscillation experiment proposal [40], consists of placing a neutrino detector at some angle with respect to the conventional neutrino beam. An “off-axis” detector records approximately the same flux of

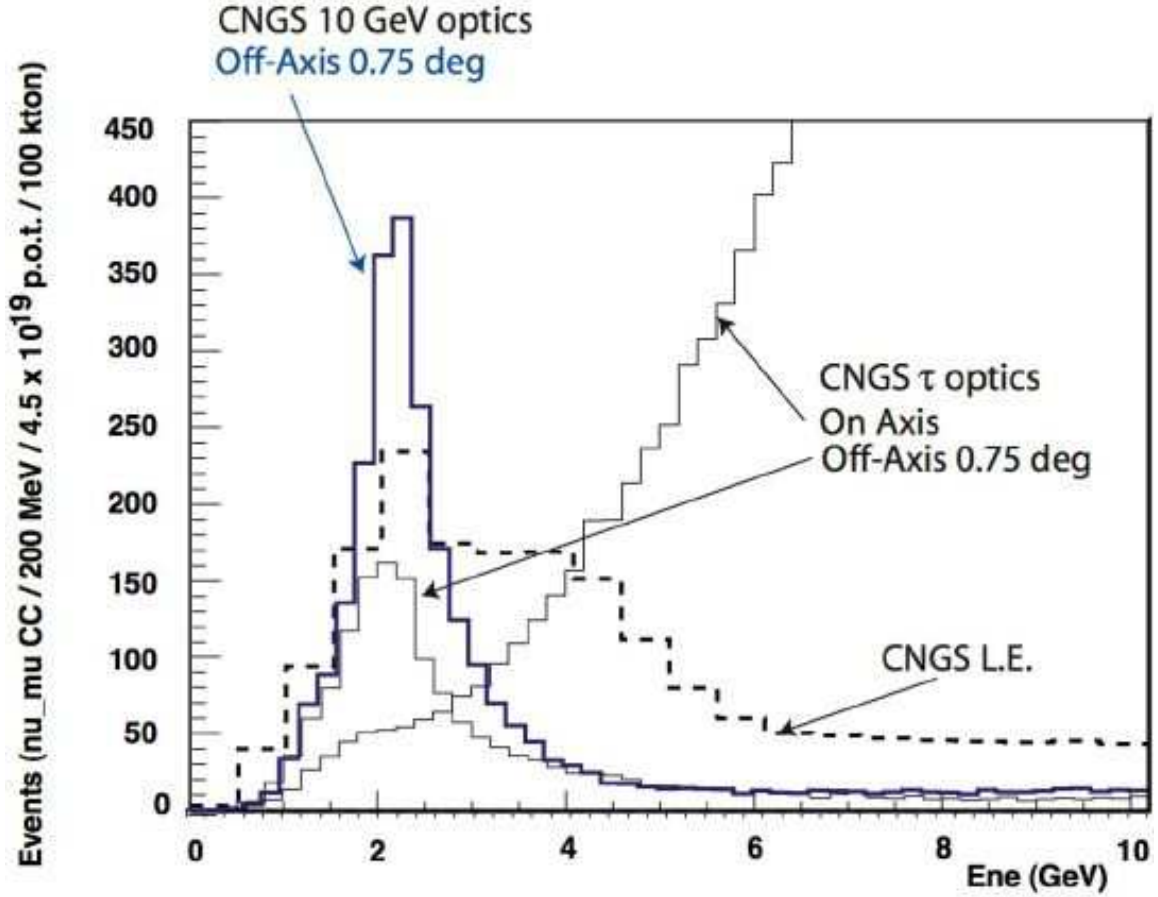


Figure 2: Comparison of ν_μ CC event spectra for on-axis and off-axis configurations in the CNGS τ and CNGS 10 GeV optics (see text). Rates normalized for comparison to a baseline of 732 km. For the off-axis configurations, events correspond to the pion peak; the selected scale of the histogram does not show the kaon peak at higher energies.

low energy neutrinos, as the one positioned “on-axis”, originating from the decays of low energy mesons. In addition, though, an “off-axis” detector records an additional contribution of low energy neutrinos from the decay of higher energy parents decaying at a finite angle.

Considering only neutrinos produced by pion and kaon decays which are the dominant contributions to muon neutrinos or antineutrinos, the neutrino energy E_ν and decay angle θ_ν with respect to the meson flight path are in the laboratory system simply correlated, because of the involved two-body decays of the type $M \rightarrow \mu\nu_\mu$, where $M = \pi, K$:

$$E_\nu(\gamma, \theta_\nu) \approx E_\nu^{max} \frac{1}{(1 + \gamma^2 \theta_\nu^2)} \quad (1)$$

where γ is the Lorentz boost of the parent meson, and E_ν^{max} is the maximum neutrino energy, i.e. $E_\nu^{max} = 0.427\gamma m_\pi$ for pions and $E_\nu^{max} = 0.954\gamma m_K$ for kaons. The neutrino energy E_ν is hence proportional to the pion energy for on-axis configuration ($\theta_\nu \equiv 0$). For off-axis configuration the derivative with respect to energy yields $dE_\nu/d\gamma \propto (1 - \gamma^2 \theta_\nu^2)/(1 + \gamma^2 \theta_\nu^2)^2$. Hence, the derivative is positive for $\gamma = 0$, it is zero when $\gamma^2 \theta_\nu^2 = 1$, and negative for $\gamma^2 \theta_\nu^2 > 1$. It tends to zero from below for $\gamma^2 \theta_\nu^2 \rightarrow \infty$. The possible neutrino energy reaches therefore a maximum

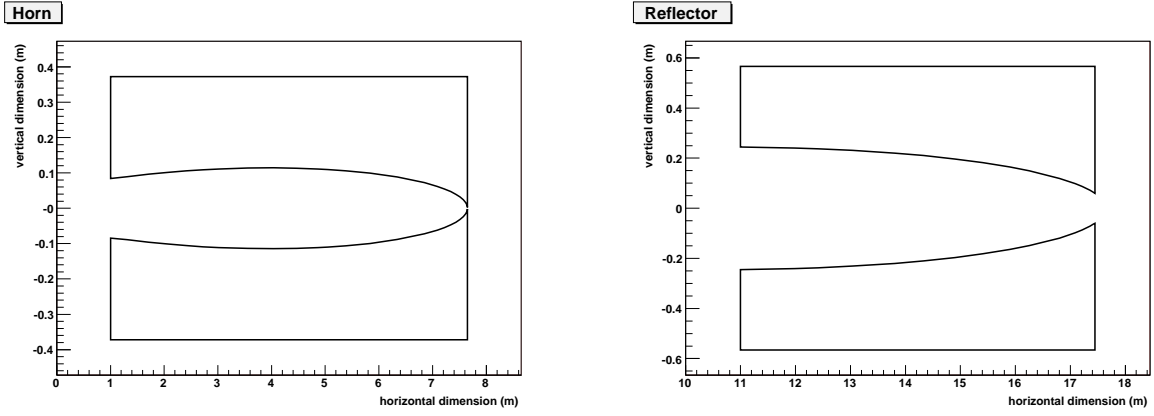


Figure 3: Geometry of horn and reflector for CNGS 10 GeV optics.

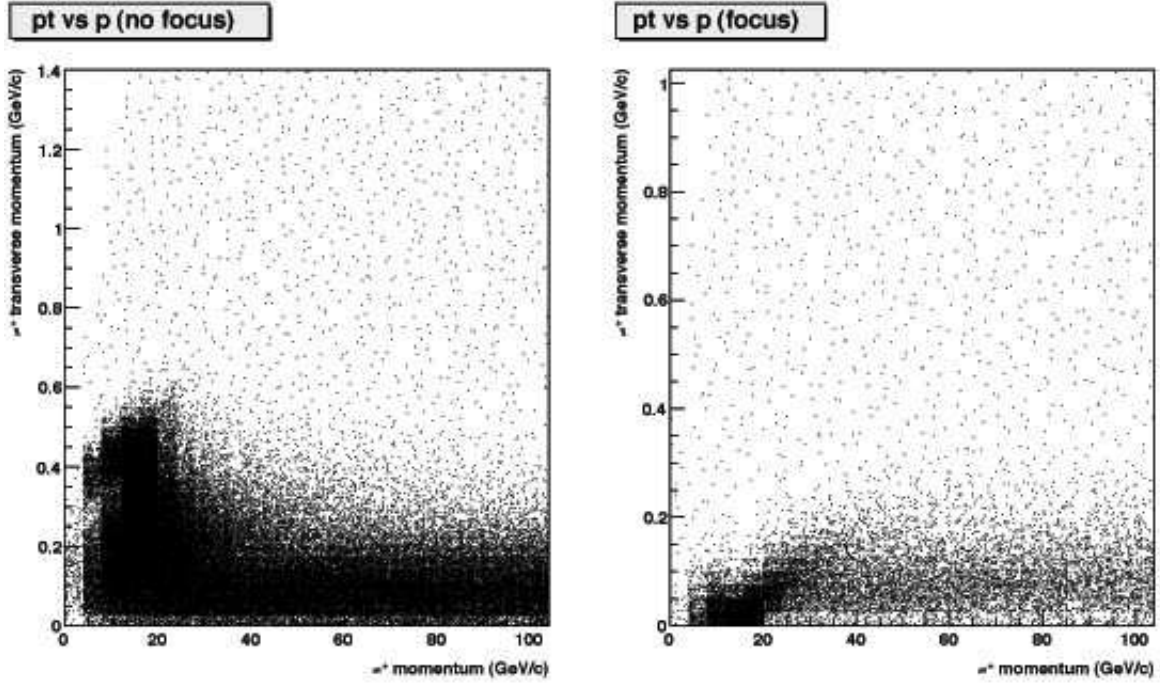


Figure 4: Distribution of momentum versus transverse momentum of pions before and after the focusing for CNGS 10 GeV optics.

value independent of the parent meson energy: for pions, $E_\nu^{highest} = 0.427m_\pi/2\theta_\nu$. Therefore, an additional attractive feature of the neutrino flux observed at the “off-axis” detector is a kinematical suppression of high energy neutrino component: detectors placed at different angles with respect to the neutrino beam direction are exposed to an intense narrow-band neutrino with the energy defined by the detector position³.

In the case of CNGS, an example of beam at 0.75° off-axis retaining the current τ -focusing

³For kaons, the maximum neutrino energy is $E_\nu^{highest} = 0.954m_K/2\theta_\nu$, which produces a neutrino flux peak at an energy about 8 times higher than for pions. The relative intensity of the pion and kaon peaks scales with the ratio of π/K production yields, which depends on the proton beam energy, and on the off-axis angle since the neutrinos produced in kaon decays are less forward peaked than those produced in pion decays.

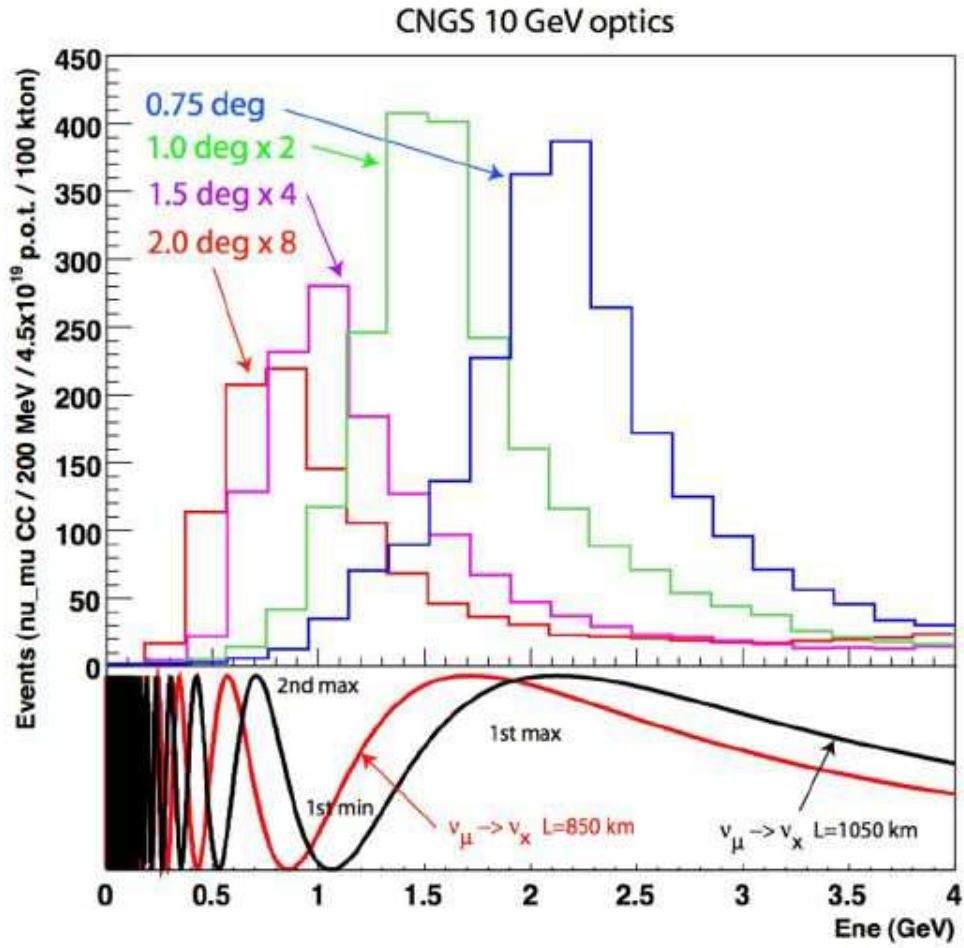


Figure 5: Expected ν_μ CC event spectra and 2 flavours oscillation probability at 850 km and 1050 km with $\Delta m^2 = 2.5 \times 10^{-3} eV^2$. The plots have been normalized for comparison to a baseline of 732 km, and the resp. 1.0° , 1.5° and 2.0° off-axis curves have been multiplied by resp. a factor 2,4, and 8. Events correspond to the pion peak; the selected scale does not show the kaon peak at higher energies.

optics is shown in Figure 2 (see curve labeled as “CNGS τ optics Off-Axis 0.75 deg”). In comparison to the on-axis CNGS L.E. the rate around 2 GeV is reduced by about a 30%. On the other hand, the tail above 2 GeV is highly suppressed as expected in the off-axis configuration.

In order to improve the flux at 2 GeV, we consider the possibility to change the CNGS optics. Since in the off-axis configuration the neutrino energy is almost independent of the parent meson energy, it is better to move towards a focalization of lower energy pions which are more abundant, compared to the CNGS τ optics which focalizes high energy pions around 35 and 50 GeV/c. We therefore propose a secondary pion focalization with momenta around 10 GeV/c.

The parameters of this adopted “CNGS 10 GeV” optics are summarized in Table 2. We started from an optics configuration similar to that of the CNGS τ and performed the following minimal changes: (a) reduced the number of rods to 8; (b) moved the horn to a distance of 100 cm; (c) recomputed the horn parabolic shape to focus 10 GeV pions (see Figure 3); (d) moved the reflector to a distance of 11 m; (e) recomputed shape of the reflector. The meson focalization and the resulting neutrino fluxes have been computed by means of a fast Monte-Carlo simulation [41] based on a particle yield parameterization [42] and a full particle transport through the focusing system and decay tunnel. The effect of the focusing on pions is shown in Figure 4. The resulting beam CNGS 10 GeV off-axis 0.75 deg is also plotted in Figure 2. In comparison to the CNGS τ optics, the neutrino spectrum energy is similar, however, a gain of almost 2 in flux can be observed.

As a final remark, we note that the CNGS 10 GeV optics optimization is rather simpler than the one of the CNGS L.E. but must be considered as preliminary. Further optimizations and improvements are possible (e.g. 3 horn optics, etc.).

For the far detector, various off-axis angles can be considered. Given the CNGS beam profile (see Figure 1) for each off-axis angle one can find a corresponding baseline; as specific examples, we compute neutrino fluxes for off-axis angles ranging from 0.5° up to 1.5° at baselines from 550 km up to 1050 km. The resulting ν_μ CC event rates, the ν_e CC beam contaminations in absence of neutrino oscillations, and the corresponding ratio of intrinsic electron to muon neutrinos are summarized in Table 3. The table is normalized to a 100 kton detector mass and an integrated intensity of 4.5×10^{19} pots. Both horn polarities have been considered. The corresponding ν_μ CC event spectra are shown in Figure 5. Events correspond to the pion peak; the selected scale of the histogram does not show the kaon peak at higher energies.

5 Neutrino oscillation with an upgraded CNGS

5.1 Analysis method

In the case of flavor oscillations among three active neutrinos, the complete expressions of the conversion probabilities for a propagation through matter (assumed of constant density) are rather complicated. In order to understand the general features of electron appearance, the oscillation probabilities can be expanded in the small parameters $\sin^2 2\theta_{13}$ and the ratio $\Delta m_{21}^2/\Delta m_{31}^2$ [43, 44]. In the case of muon to electron neutrino transitions, one has $P(\nu_\mu \rightarrow \nu_e) \equiv P_{\mu e}(\Delta, \hat{A}, \alpha, \theta_{ij}, \delta_{\text{CP}}) = P_{e\mu}(\Delta, \hat{A}, \alpha, \theta_{ij}, -\delta_{\text{CP}}) = P_{\bar{\mu}\bar{e}}(\Delta, -\hat{A}, \alpha, \theta_{ij}, -\delta_{\text{CP}})$, with $\alpha \equiv \Delta m_{21}^2/\Delta m_{31}^2 \sim \pm 0.03$ (the $\text{sgn}(\alpha)$ is determined by the neutrino mass hierarchy), $\Delta \equiv (1/4)\Delta m_{31}^2 L/E_\nu$ and $\hat{A} \equiv 2\sqrt{2}G_F n_e E/\Delta m_{31}^2 \simeq 7.56 \times 10^{-5} \text{ eV}^2 \rho(g/cm^3) E(\text{GeV})/\Delta m_{31}^2$, and $P_{e\mu}$ is

$$P_{e\mu}(\Delta, \hat{A}, \alpha, \theta_{ij}, \delta_{\text{CP}}) \simeq \sin^2 2\theta_{13} T_1 + \alpha \sin 2\theta_{13} T_2 + \alpha \sin 2\theta_{13} T_3 + \alpha^2 T_4, \quad (2)$$

Off-axis CNGS						
	neutrino horn polarity			antineutrino horn polarity		
Distance/ Off-axis angle	ν_μ CC ($\bar{\nu}_\mu$ CC)	ν_e CC ($\bar{\nu}_e$ CC)	$(\nu_e + \bar{\nu}_e) /$ $(\nu_\mu + \bar{\nu}_\mu)$	ν_μ CC ($\bar{\nu}_\mu$ CC)	ν_e CC ($\bar{\nu}_e$ CC)	$(\nu_e + \bar{\nu}_e) /$ $(\nu_\mu + \bar{\nu}_\mu)$
τ optics , 400 GeV/c protons						
550 km 0.75 deg	2282 (335)	118 (20)	4.3 %	784 (1043)	43 (42)	4.7 %
800 km 0.5 deg	3761 (185)	65 (10.7)	1.9 %	436 (1400)	24 (24)	2.6 %
850 km 0.75 deg	1206 (140)	49 (8.4)	4.3 %	327 (436)	18.2 (17.5)	4.7 %
900 km 1 deg	607 (97)	31 (6.1)	5.3 %	225 (214)	13.1 (11.4)	5.6 %
1050 km 1.5 deg	246 (34)	9.7 (2.5)	4.4 %	79 (84)	5.4 (3.7)	5.6 %
10 GeV optics , 400 GeV/c protons						
550 km 0.75 deg	4706 (341)	111 (22)	2.6 %	862 (1732)	52 (42)	3.6 %
800 km 0.5 deg	5687 (275)	67 (11.9)	1.3 %	678 (2167)	28 (27)	1.9 %
850 km 0.75 deg	1970 (142)	47 (9.2)	2.6 %	361 (725)	22 (17.6)	3.6 %
900 km 1 deg	919 (87)	31 (6.6)	3.8 %	223 (321)	15.6 (11.7)	5.0 %
1050 km 1.5 deg	340 (37)	12.1 (3.3)	4.1 %	154 (100)	8.2 (4.6)	5.0 %

Table 3: Number of events calculated for $4.5E+19$ p.o.t. and a detector mass of 100 kton. A upper cut on the neutrino energy has been set at 10 GeV.

where the individual terms are of the form

$$T_1 = \sin^2 \theta_{23} \frac{\sin^2[(1 - \hat{A})\Delta]}{(1 - \hat{A})^2}, \quad (3)$$

$$T_2 = \sin \delta_{\text{CP}} \sin 2\theta_{12} \sin 2\theta_{23} \sin \Delta \frac{\sin(\hat{A}\Delta)}{\hat{A}} \frac{\sin[(1 - \hat{A})\Delta]}{(1 - \hat{A})}, \quad (4)$$

$$T_3 = \cos \delta_{\text{CP}} \sin 2\theta_{12} \sin 2\theta_{23} \cos \Delta \frac{\sin(\hat{A}\Delta)}{\hat{A}} \frac{\sin[(1 - \hat{A})\Delta]}{(1 - \hat{A})}, \quad (5)$$

$$T_4 = \cos^2 \theta_{23} \sin^2 2\theta_{12} \frac{\sin^2(\hat{A}\Delta)}{\hat{A}^2}. \quad (6)$$

It is well documented in the literature [45, 46, 47] that the most challenging task for next generation long baseline experiments, is to unfold the unknown oscillation parameters $\sin^2 2\theta_{13}$, δ_{CP} and mass hierarchy, $\text{sgn}(\Delta m_{31}^2)$, from the measurement of the oscillation signal binned in energy, to resolve the so-called problems of “correlations” and “degeneracy”. The most important experimental aspects here are the beam profile (e.g. the ability to cover with sufficient statistics the 1st maximum of the oscillation, the 1st minimum, and the 2nd maximum), the visible energy resolution of the detector, with which the neutrino energy can be reconstructed, and the spectrum of the misidentified background (e.g. π^0 spectrum, typ. populating mostly at lower energies, in the region of 2nd maximum and below).

For example, this can be intuitively understood from looking at the oscillation probabilities at different energies for normal and inverted mass hierarchy for varying δ_{CP} -angles. These oscillation probabilities for neutrinos and antineutrinos as parametric plots as a function of the δ_{CP} -phase are plotted in Figure 6 for a baseline of 850 km and Figure 7 for 1050 km.

If we consider the problem of determination of the mass hierarchy, we observe that the ellipses for normal and inverted hierarchy can often lead to the same probabilities for both neutrinos and antineutrinos if the δ_{CP} phase is rotated by an appropriate angle. For example, if we take a baseline of 850 km and a neutrino energy of 1 GeV, the phase $\delta_{\text{CP}} = 90^\circ$ with normal hierarchy can be confused with $\delta_{\text{CP}} = 270^\circ$ of the inverted hierarchy (see Figure 6). In absence of knowledge of the δ_{CP} -phase, the mass hierarchy can therefore not be disentangled.

However, the graphs show that the energy dependence of the oscillation probabilities, and hence the good energy resolution of the detector and the “wideness” of the neutrino beam spectrum (to cover 1st maximum, the 1st minimum, and 2nd maximum) help solving these ambiguities. In addition, as is illustrated by Figures 6 and 7, measurements at different baselines can provide a solution to the correlation and degeneracy.

We note that the 1st minimum is a privileged point in the spectrum, since by definition it does not depend on θ_{13} and δ_{CP} . It therefore as a fixed point driven by the solar oscillation $\sin^2 2\theta_{12}, \Delta m_{21}^2$ (in fact, given the E/L 's involved, the probability essentially depends on the product of the two quantities).

In order to address the above mentioned issues in a well-defined framework, we computed the sensitivities to neutrino oscillations with the GLoBES software [48]. As input (or so called true) values for the neutrino oscillation parameters, we use, unless stated otherwise, the following standard figures where the errors are assumed to be the relevant ones given the timescale of the present experimental programme:

$$\begin{aligned} \Delta m_{31}^2 &= (2.5^{+0.025}_{-0.025}) \cdot 10^{-3} \text{ eV}^2 & \sin^2 \theta_{23} &= 0.5^{+0.008}_{-0.008}, \\ \Delta m_{21}^2 &= (7.0^{+0.7}_{-0.7}) \cdot 10^{-5} \text{ eV}^2 & \sin^2 \theta_{12} &= 0.31^{+0.06}_{-0.05}, \\ & & \sin^2 \theta_{13} &= 0 \quad \delta_{\text{CP}} = 0. \end{aligned} \quad (7)$$

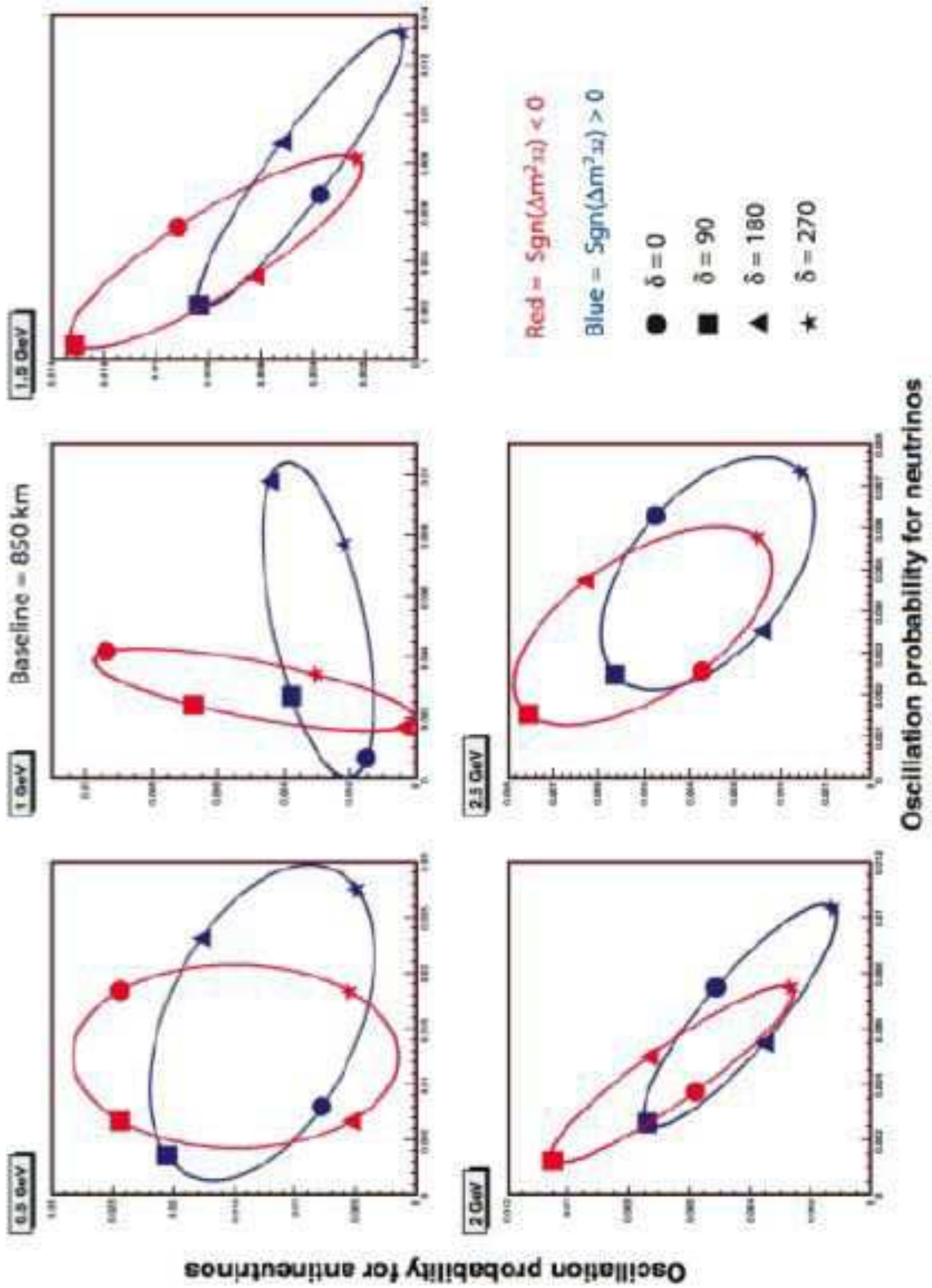


Figure 6: Parametric plot of probabilities of neutrinos vs antineutrinos for different neutrino energies as a function of the δ_{CP} -phase for a baseline of 850 km, computed for $\sin^2 2\theta_{13} = 0.01$.

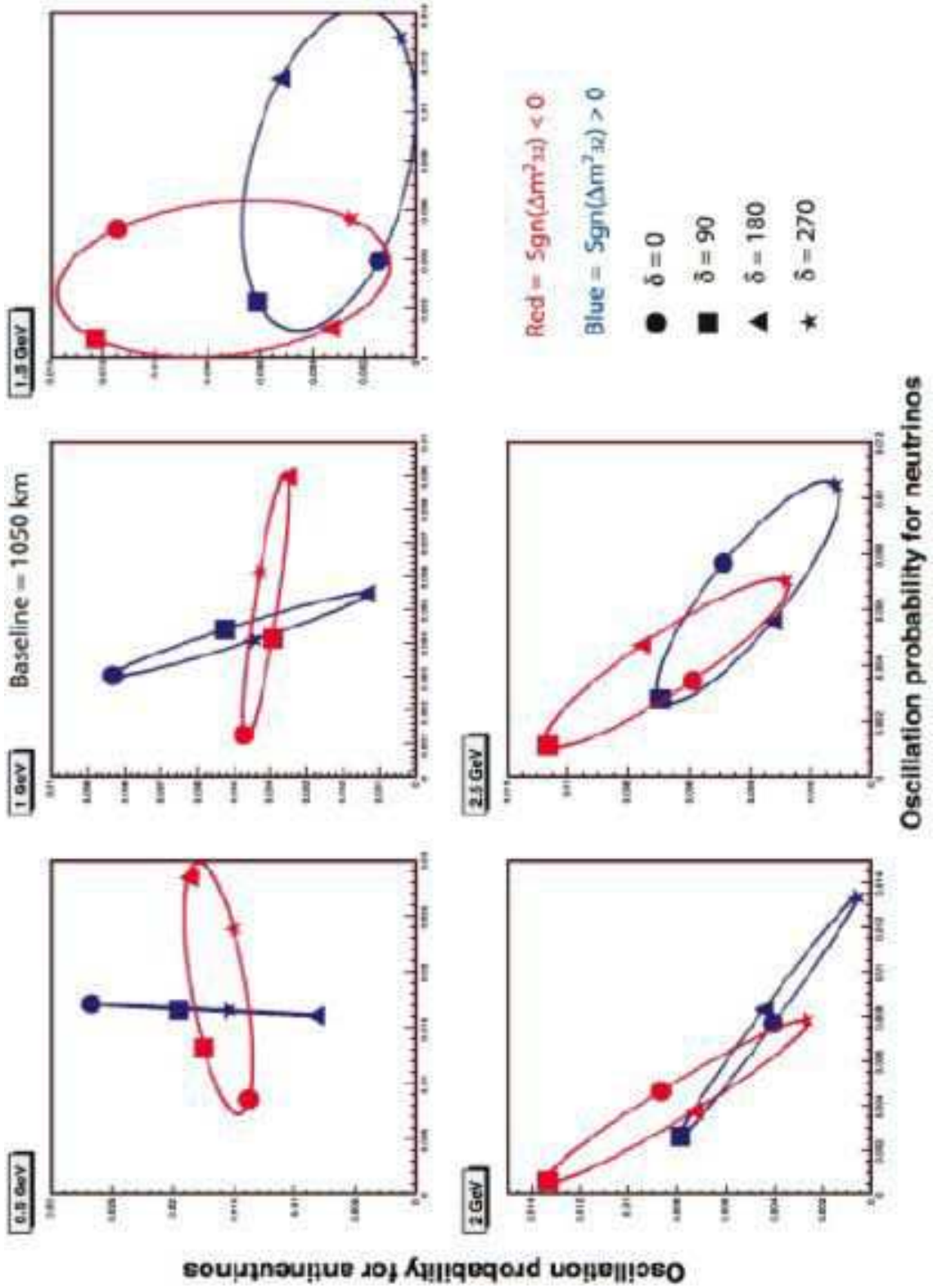


Figure 7: Parametric plot of probabilities of neutrinos vs antineutrinos for different neutrino energies as a function of the δ_{CP} -phase for a baseline of 1050 km, computed for $\sin^2 2\theta_{13} = 0.01$.

All calculations generally assume a normal mass hierarchy as input, whereas the fit always extends to the case of an inverted hierarchy. As shown in Ref. [49], although normal and inverted hierarchy are not totally symmetric, qualitatively no fundamental differences in the sensitivities are expected for the two cases, since we always assume the possibility to run the horn polarities in positive and negative modes. In the case of a true inverted hierarchy, the antineutrino polarity should be favored in integrated intensity to compensate for the lower antineutrino cross-section compared to neutrinos.

The errors on the input parameters are as important as their central values, since the sensitivity to flavor oscillations will be estimated by letting all parameters free within priors given by their errors, in the minimization of the χ^2 . In addition, we include matter density uncertainties at the level of 5% [50, 51], uncorrelated between different baselines.

In order to obtain conservative yet realistic results, we include the $\text{sgn}(\Delta m_{31}^2)$ -degeneracy and the $(\theta_{13}, \delta_{\text{CP}})$ -degeneracy, whereas the octant degeneracy ($\theta_{23} \rightarrow \pi/2 - \theta_{23}$) does not appear since we limit ourselves to maximal mixing.

The number of events as a function of energy expected in our design detector is computed for a given set of oscillation parameters. We assume a $\simeq 90\%$ signal efficiency, a systematic error on the ν_e background of 5%, a negligible π^0 NC background (compared to intrinsic ν_e), and no charge discrimination (for each channel, neutrinos and antineutrinos CC events are added). Once the event rates are computed and binned in energy steps of 100 MeV, the calculation of the χ^2 function assuming Poisson distributions is performed, and including the systematic errors using the pull approach [48]. During the χ^2 calculation, all oscillation parameters and the matter density are let free within their priors and the function is minimized at each considered point to fully include direct degeneracies. As mentioned above, explicit “clone” solutions (e.g. opposite mass hierarchy) are included as well, as discreet χ^2 tests starting with appropriate input values ($\Delta m^2 \rightarrow -\Delta m^2$) and repeating the minimization procedure for the potential clone solution. In general, the χ^2 values obtained by the above procedure are converted into confidence levels by using the χ^2 distribution for two degrees of freedom in the $(\sin^2 2\theta_{13}, \delta_{\text{CP}})$ -plane. We will also use the idea of CP fraction, the definition of which is e.g. provided in Figure 3 of Ref. [52].

5.2 Optimal off-axis angles

As we discussed above, the neutrino beam spectrum in an off-axis configuration is sharply peaked at a given neutrino energy and the high energy component is highly suppressed (neglecting the kaon peak). The position of the peak is directly related to the chosen off-axis angle. Given the rather narrow nature of the obtained beam spectrum, it is important to choose the location appropriately.

In order to maximize the flux at the first maximum of the oscillation probability, one must choose the energy of the neutrino E and the baseline L such that $\Delta \equiv 1/4\Delta m_{31}^2 L/E_\nu \simeq \pi/2$. Similarly, in order to observe the first minimum and 2nd maximum, one needs $\Delta \simeq \pi, 3\pi/2$. In general,

$$\frac{1}{4}\Delta m_{31}^2 \frac{L}{E_\nu^\phi} \simeq \phi \longrightarrow E_\nu^\phi \simeq \frac{1}{4}\Delta m_{31}^2 \frac{L}{\phi}, \quad \phi = \frac{\pi}{2}(1^{\text{st}} \text{ max}), \pi(1^{\text{st}} \text{ min}), \frac{3\pi}{2}(2^{\text{nd}} \text{ max}) \quad (8)$$

Oscillations beyond the 2nd maximum are hardly accessible in the present configuration given the detector visible energy resolution.

This last equation can be combined with Eq. 1 to define the *optimal off-axis angle* $\theta_\nu^{\text{opt},\phi}$:

$$E_\nu^\phi \simeq \frac{1}{4}\Delta m_{31}^2 \frac{L}{\phi} \simeq E_\nu^{\text{max}} \frac{1}{(1 + \gamma^2 \theta_\nu^2)} \longrightarrow \theta_\nu^{\text{opt},\phi} \simeq \frac{1}{\gamma} \left(\frac{4E_\nu^{\text{max}} \phi}{\Delta m_{31}^2 L} - 1 \right)^{1/2} \quad (9)$$

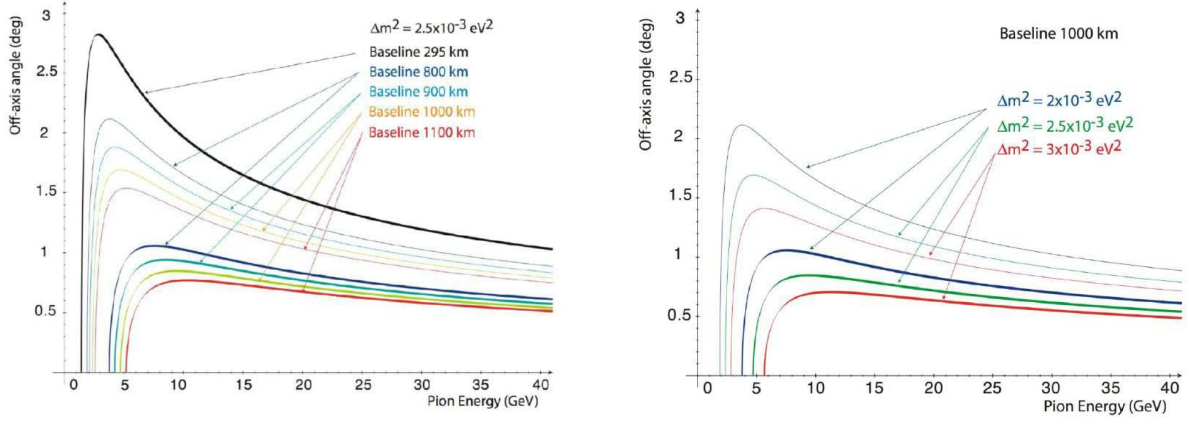


Figure 8: (left) Optimal maximum (thick lines) and minimum (thin lines) off axis angles as a function of pion energy for $\Delta m^2 = 2.5 \times 10^{-3} \text{eV}^2$ and different baselines. (right) Optimal maximum (thick lines) and minimum (thin lines) off axis angles as a function of pion energy at a baseline of 1000 km for different Δm^2 .

The optimal 1st maximum (thick lines) and 1st minimum (thin lines) off axis angle as a function of pion energy for $\Delta m^2 = 2.5 \times 10^{-3} \text{eV}^2$ and the baselines 295, 800, 900, 1000, and 1100 km are shown in Figure 8 (left). Similar curves for a fixed baseline of 1000 km and for $\Delta m^2 = (2, 2.5, 3) \times 10^{-3} \text{eV}^2$ are shown in Figure 8 (right).

The optimal off-axis angles to observe the 1st maximum is as expected almost independent of the pion energy (for pions above ≈ 10 GeV) and lies in the range 0.5° and 1.0° off-axis for baselines within 800 and 1000 km. Similarly, optimal off-axis angles to observe the 1st minimum obey same properties and are in the range 1.0° and 1.5° off-axis. We note that for a much shorter baseline, e.g. 295 km as in the case Tokai-Kamioka, the optimal off-axis angle is much larger, and depends more strongly on the pion energy. Similar curves can be computed for the 2nd maximum.

For this document, we will therefore consider two off-axis angles: (a) an OA0.75 at a baseline of 850 km (see Figure 1 and Table 3) to optimize the rate at the 1st maximum, optimally tuned for the best $\sin^2 2\theta_{13}$ sensitivity; (b) an OA1.5 at a baseline of 1050 km to increase the flux at the second maximum and 1st minimum (see Figure 5), in order to improve the sensitivity to the CP-violation and mass hierarchy.

5.3 Discovery of $\nu_\mu \rightarrow \nu_e$ and sensitivity to CP-phase and mass hierarchy with one detector at 850 km, OA0.75

We can now combine all the ingredients presented in the previous sections to compute the physics potential of a given detector configuration. The detector of 100 kton is located at a distance of 850 km from CERN in an off-axis configuration of 0.75° . The expected number of events is presented in Table 3. We assume 5 years of running in the neutrino horn polarity mode, plus 5 additional years in the antineutrino polarity mode. As already mentioned, the actual integrated luminosity in neutrino and antineutrino polarities will depend on hints on the mass hierarchy. For a normal (resp. an inverted) mass hierarchy, the neutrino (resp. antineutrino) horn polarity should be favored.

5.3.1 Sensitivity to $\sin^2 2\theta_{13}$

In order to discover a non-vanishing $\sin^2 2\theta_{13}$, the hypothesis $\sin^2 2\theta_{13} \equiv 0$ must be excluded at the given C.L. As input, a true non-vanishing value of $\sin^2 2\theta_{13}$ is chosen in the simulation and a fit with $\sin^2 2\theta_{13} = 0$ is performed, yielding the “discovery” potential⁴. This procedure is repeated for every point in the $(\sin^2 2\theta_{13}, \delta_{CP})$ plane.

The corresponding sensitivity to discover θ_{13} in the true $(\sin^2 2\theta_{13}, \delta_{CP})$ plane at 90% C.L. and 3σ is shown in Figure 9. The left-most dashed curve corresponds to neutrino and antineutrino polarity runs, with all oscillation parameters fixed and no systematic error at 90 %C.L. The corresponding curves for neutrino run only or antineutrino run only are also shown as dashed curves. The sensitivities leaving all other oscillation parameters free in the minimization is also shown as dashed curves. Corresponding sets of sensitivities at 3σ are displayed as continuous lines.

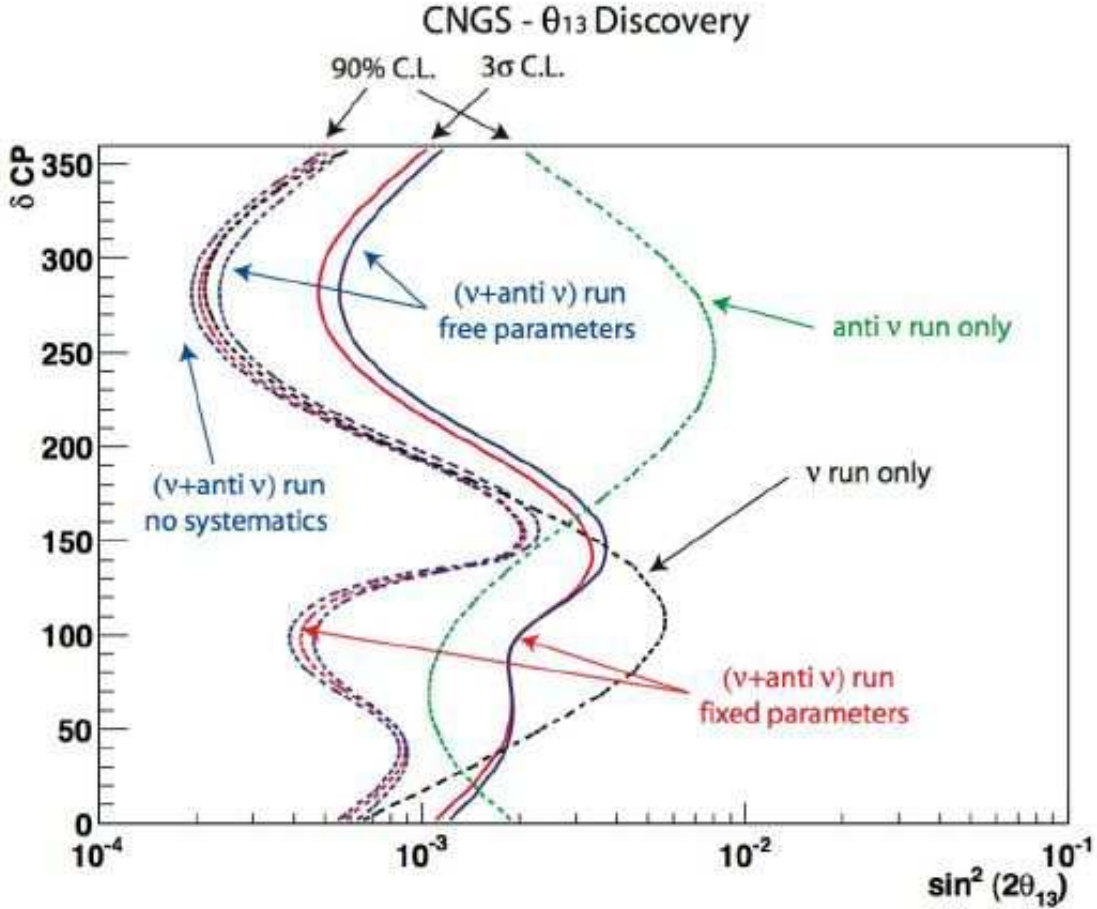


Figure 9: Sensitivity to discover θ_{13} in the true $(\sin^2 2\theta_{13}, \delta_{CP})$ plane. The left-most dashed curve corresponds to neutrino and antineutrino polarity runs, with all oscillation parameters fixed and no systematic error at 90 %C.L. The corresponding curves for neutrino run only or antineutrino run only are also shown as dashed curves. The sensitivity leaving all other oscillation parameters free in the minimization is also shown as dashed curves. Corresponding sets of sensitivities at 3σ are displayed as continuous lines.

⁴We note that “discovery” is not exactly the same as giving $\sin^2 2\theta_{13} = 0$ as true input and fitting $\sin^2 2\theta_{13} \neq 0$ (“sensitivity”), however results are rather similar.

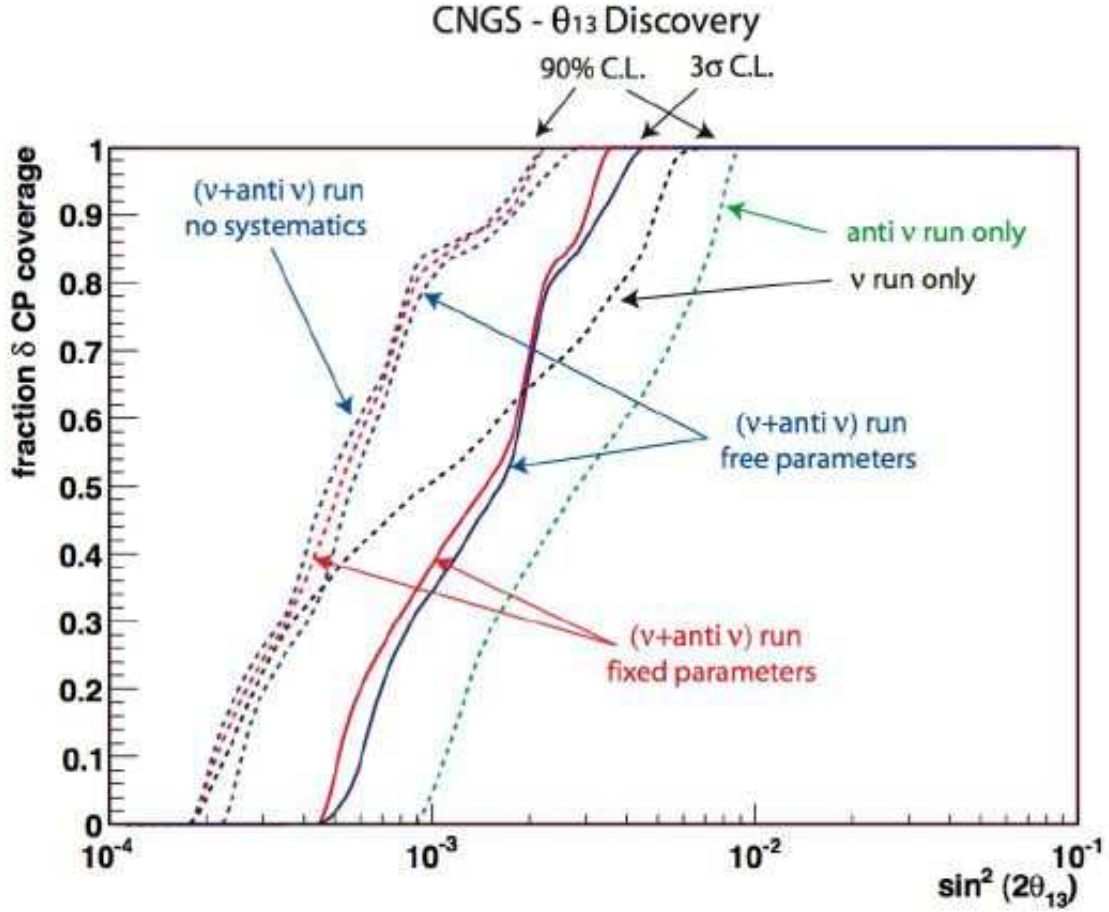


Figure 10: Sensitivity to discover θ_{13} : the fraction of δ_{CP} coverage as a function of $\sin^2 2\theta_{13}$ corresponding to result plotted in Figure 9.

From these graphs, it is quite apparent that sensitivities down to $\sin^2 2\theta_{13} \lesssim 0.001$ are achieved at the 90% C.L. The coupling of the neutrino and antineutrino runs gives the more uniform sensitivity as a function of the true δ_{CP} . Without antineutrino run, the sensitivity obtained with neutrinos only exhibits the characteristic “S”-shape as a function of δ_{CP} .

The inclusion of all correlations (“free parameters” on the graph) does not appreciably degrade the sensitivity as expected since in absence of signal the dependence to the other oscillation parameters is mild.

The same information displayed in terms of the fraction of true CP phase is shown in Figure 10. It shows that a non-vanishing θ_{13} can be discovered with 100% probability for $\sin^2 2\theta_{13} > 0.004$ at 3σ .

5.3.2 Sensitivity to CP-violation

By definition, the CP-violation in the lepton sector can be said to be discovered if the CP-conserving values, $\delta_{CP} = 0$ and $\delta_{CP} = \pi$, can be excluded at a given C.L. The reach for discovering CP-violation is computed choosing a “true” value for δ_{CP} ($\neq 0$) as input at different true values of $\sin^2 2\theta_{13}$ in the $(\sin^2 2\theta_{13}, \delta_{CP})$ -plane, and for each point of the plane calculating the corresponding event rates expected in the experiment. This data is then fitted with the two

CP-conserving values $\delta_{\text{CP}} = 0$ and $\delta_{\text{CP}} = \pi$, leaving all other parameters free (including δ_{CP} and $\sin^2 2\theta_{13}$!). The opposite mass hierarchy is also fitted and the minimum of all cases is taken as final χ^2 .

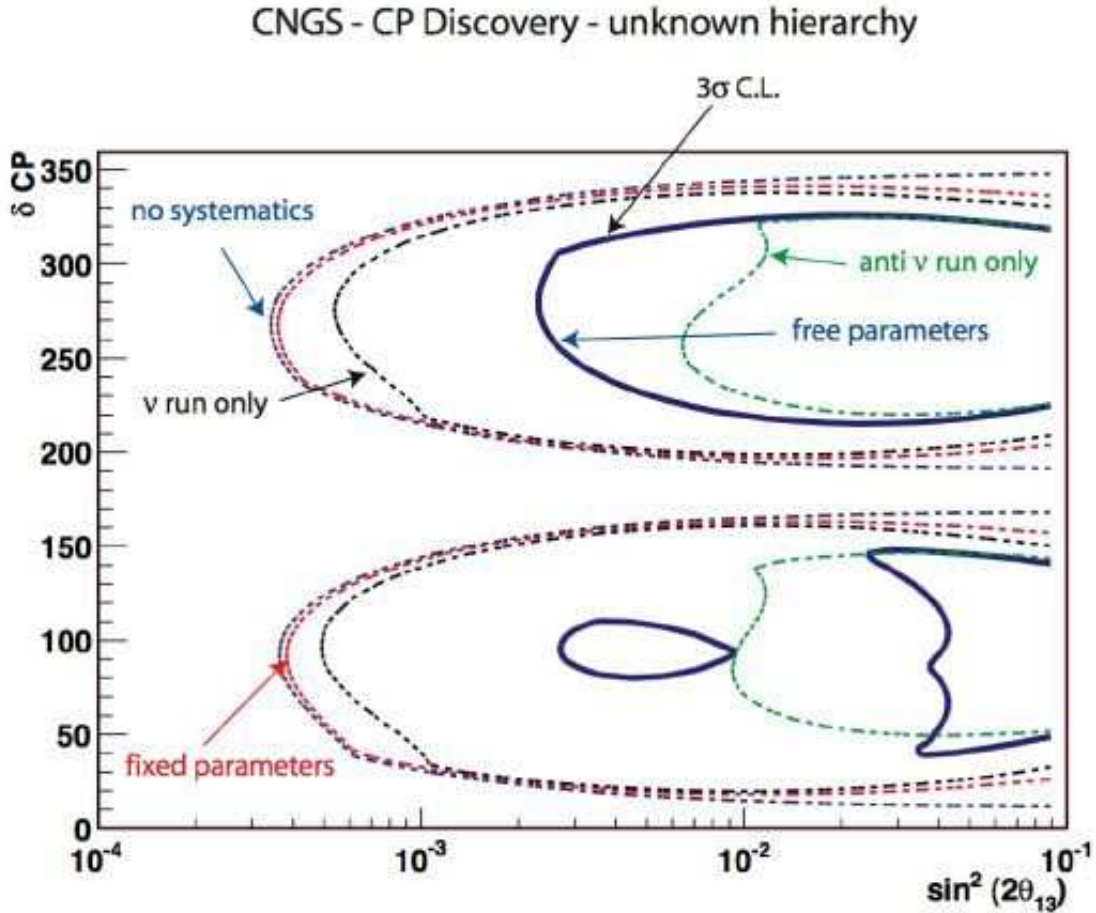


Figure 11: Sensitivity to discover CP-violation in the true $(\sin^2 2\theta_{13}, \delta_{\text{CP}})$ plane. The left-most dashed curve corresponds to neutrino and antineutrino polarity runs, with all oscillation parameters fixed and no systematic error at 90 %C.L. The corresponding curves for neutrino run only or antineutrino run only are also shown as dashed curves. The 3σ sensitivity including correlations and degeneracy (leaving all other oscillation parameters free in the minimization) is displayed as a continuous line.

The corresponding sensitivity to discover CP-violation in the true $(\sin^2 2\theta_{13}, \delta_{\text{CP}})$ plane is shown in Figure 11. The left-most dashed curve corresponds to neutrino and antineutrino polarity runs, with all oscillation parameters fixed and no systematic error at 90 %C.L. The corresponding curves for neutrino run only or antineutrino run only are also shown as dashed curves. The 3σ sensitivity including correlations and degeneracy (leaving all other oscillation parameters free in the minimization) is displayed as a continuous line.

At the considered baseline of 850 km, matter effects are at the level of 30 %, hence it can be difficult to detect and untangle this effect from CP-phase induced asymmetries. Indeed, for certain combinations of true $\sin^2 2\theta_{13}$ and δ_{CP} , it is possible to fit the data with the wrong mass hierarchy and a rotated δ_{CP} , an effect labelled as π -transit [49].

This effect is strongly affecting the sensitivity to discover CP-violation around a true $\delta_{\text{CP}} \approx 90^\circ$ when the mass hierarchy is unknown. This is clearly seen in the graphs: when

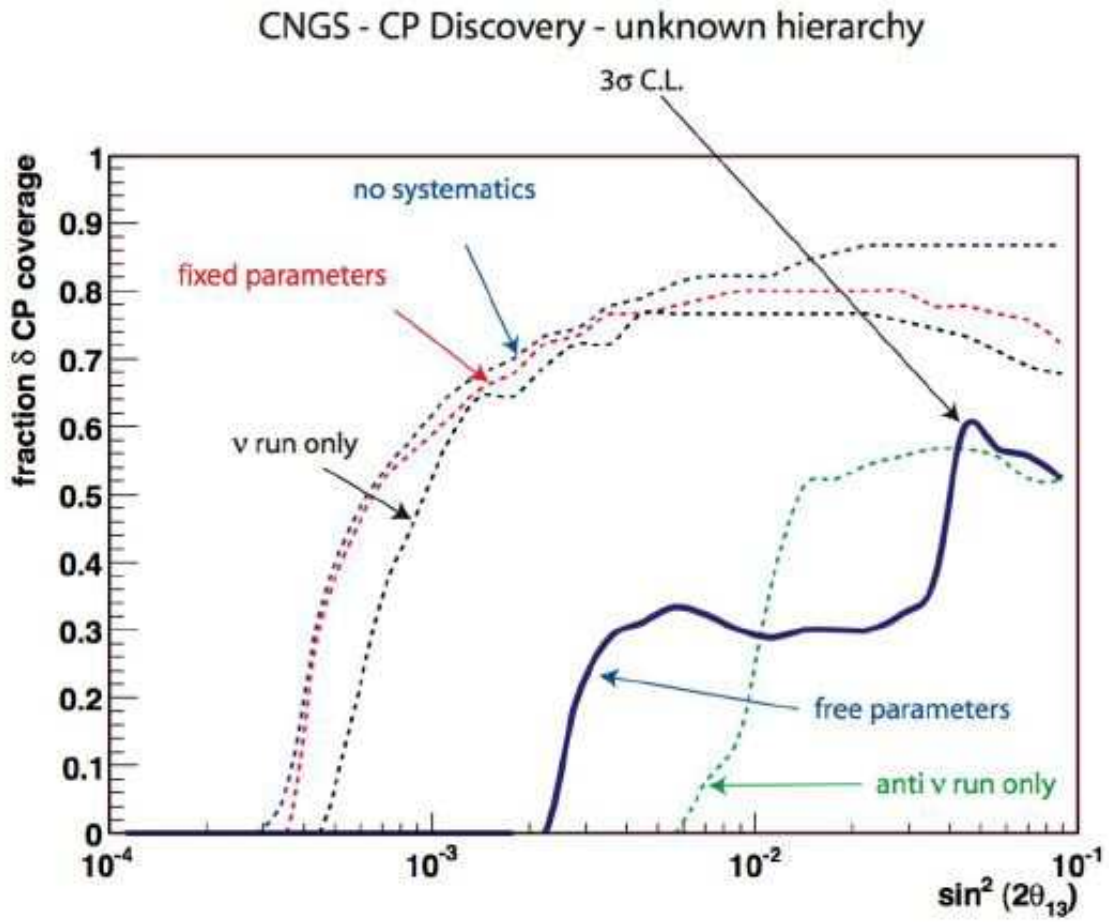


Figure 12: Sensitivity to discover CP-violation: the fraction of δ_{CP} coverage as a function of $\sin^2 2\theta_{13}$ corresponding to result plotted in Figure 11.

the parameters are fixed, the sensitivity to CP-violation at the 90% C.L. is symmetric above and below the line determined by $\delta_{\text{CP}} = 180^\circ$ and extends down to $\sin^2 2\theta_{13} \lesssim 0.001$. However, when the parameters are let free and the clone solution with opposite mass hierarchy is fitted as well, the sensitivity at true $\delta_{\text{CP}} \approx 90^\circ$ is only $\sin^2 2\theta_{13} \approx 0.04$ at 3σ -level, with a small island around $\sin^2 2\theta_{13} \approx 0.005$ where CP-violation can be discovered at 3σ even for $\delta_{\text{CP}} \approx 90^\circ$.

Running without antineutrinos would worsen the sensitivity even more, as observable from the corresponding dashed curve on the graph labeled “anti ν run only”. More antineutrino horn polarity running would improve the sensitivity in this region.

The same information displayed in terms of the fraction of true CP phase is shown in Figure 12. Defined as the possibility to exclude the CP-conserving values, $\delta_{\text{CP}} = 0$ and $\delta_{\text{CP}} = \pi$, at a given C.L., the fraction of true CP that can be discovered at 3σ reaches about 80% with *fixed oscillation parameters* for $\sin^2 2\theta_{13} \gtrsim 0.004$, however this result is strongly spoiled as expected by the correlations and the mass hierarchy degeneracy.

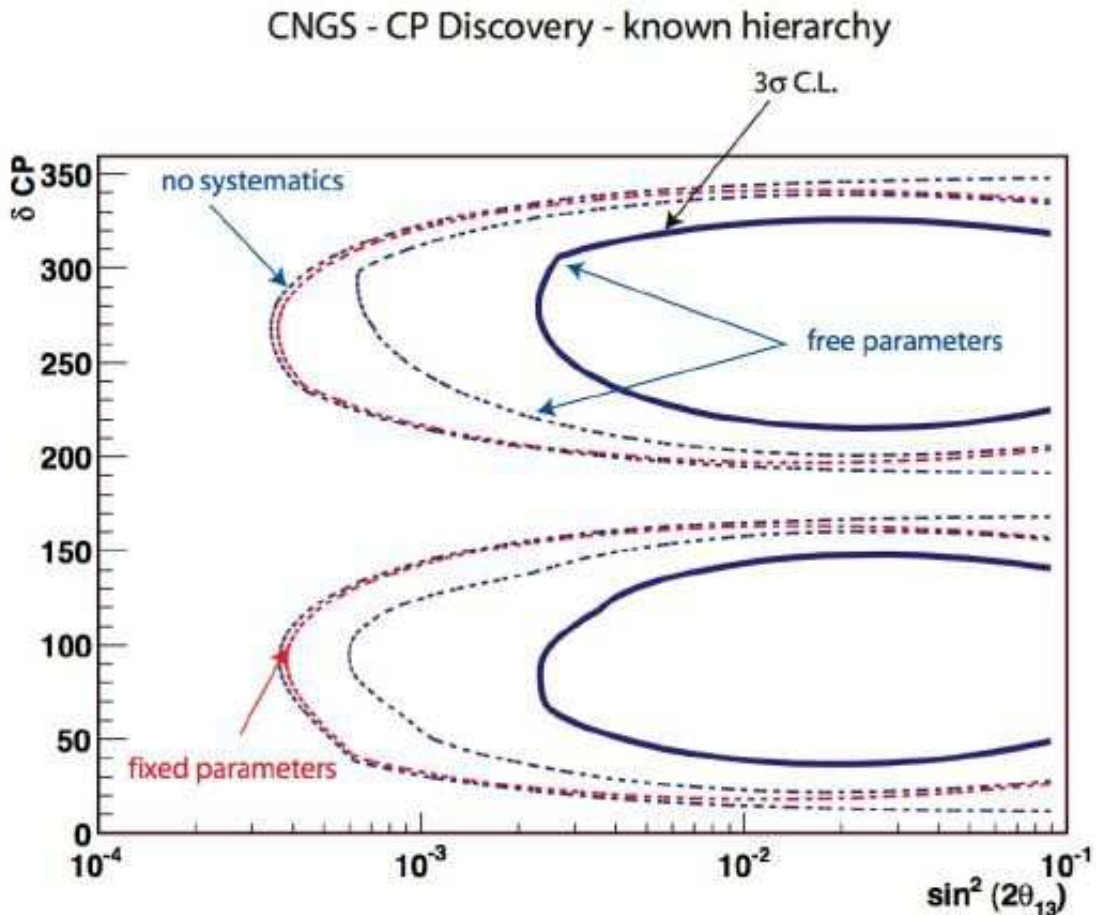


Figure 13: Same as Figure 11 with parameter correlations but without mass hierarchy degeneracy (see text).

In order to appreciate the effect of the mass hierarchy degeneracy, we repeated our calculations leaving in all correlations but assuming a normal mass hierarchy (of course, knowing that the true mass hierarchy is also normal). The results graphs are presented in Figures 13 and 14. In this case, the π -transit problem is improved and the sensitivity for $\delta_{\text{CP}} > 180^\circ$ and

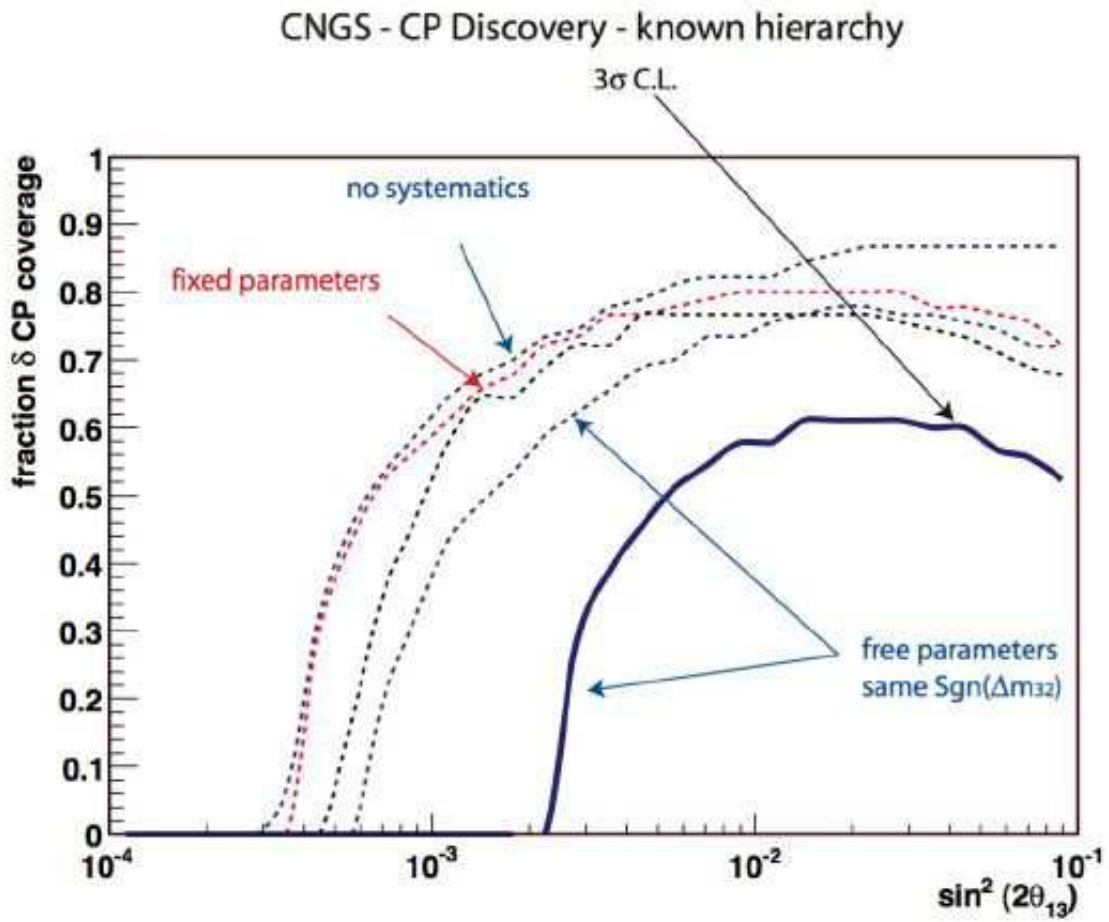


Figure 14: Same as Figure 12 with parameter correlations but without mass hierarchy degeneracy (see text).

$\delta_{\text{CP}} < 180^\circ$ are similar. If the mass hierarchy was known, CP-violation could be discovered at 3σ for $\sin^2 2\theta_{13} \gtrsim 0.003$.

The fraction of true CP that can be discovered at 3σ is still about 80% with *fixed oscillation parameters* for $\sin^2 2\theta_{13} \gtrsim 0.004$. At 3σ it reaches about 60% with free parameters for $\sin^2 2\theta_{13} \gtrsim 0.01$, degraded by the result of the inclusion of the parameter correlations.

As expected the baseline of 850 km is not very effective to determine the mass hierarchy and unfortunately the sensitivity to CP-violation is affected by it when the proper correlations and corresponding degeneracy are included in the fit. However, the rate at 850 km is sufficient to look for electron appearance down to $\sin^2 2\theta_{13} \gtrsim 0.001$.

5.3.3 Sensitivity to mass hierarchy

In order to determine the mass hierarchy to a given C.L., the opposite mass hierarchy must be excluded. A point in parameter space with normal hierarchy is therefore chosen as true value and the solution with the smallest χ^2 value with inverted hierarchy has to be determined by global minimization of the χ^2 function leaving all oscillation parameters free within their priors.

The sensitivity to exclude inverted mass hierarchy in the true ($\sin^2 2\theta_{13}, \delta_{\text{CP}}$) plane is shown in Figure 15. The left-most dashed curve corresponds to neutrino and antineutrino polarity runs, with all oscillation parameters fixed and no systematic error at 90 %C.L. The corresponding curves for neutrino run only or antineutrino run only are also shown as dashed curves. The sensitivity leaving all other oscillation parameters free in the minimization is also shown as dashed curves. The corresponding sensitivity at 3σ including correlations and degeneracy is displayed as a continuous line.

Because of a similar phenomenon as in the case of the discovery of CP-violation, the sensitivity to exclude the inverted mass hierarchy is affected the the correlations with the other oscillation parameters, in particular, the a priori unknown δ_{CP} -phase. This effect is readily seen in the graph where mass hierarchy could be determined at 90% C.L. for $\sin^2 2\theta_{13} \gtrsim 0.001$ with fixed parameters, however, when correlations are included, the sensitivity is greatly reduced to $\sin^2 2\theta_{13} \gtrsim 0.01$.

The same information displayed in terms of the fraction of true CP phase is shown in Figure 16. In terms of fraction of true CP coverage, the determination of the mass hierarchy with coverage $> 50\%$ is reached only for $\sin^2 2\theta_{13} \gtrsim 0.03$ at 3σ .

5.4 Sensitivity to mass hierarchy with one detector at 1050 km, OA1.5

We have seen in the previous section that the configuration with a 100 kton detector at 850 km at an off-axis angle of 0.75° is optimal given the statistics to search for small values of θ_{13} down to $\sin^2 2\theta_{13} \lesssim 0.001$ at 3σ .

However, because of the rather modest baseline, the effects of CP-violation and matter cannot be uniquely disentangled, and the sensitivity to discover CP-violation or to determine the mass hierarchy is strongly affected by parameter correlations and clone solution degeneracy.

In order to improve on the sensitivity on CP-violation and mass hierarchy at the cost of sensitivity to θ_{13} , we consider in the following a configuration with a detector of mass 100 kton located at a longer baseline of 1050 km and at a larger off-axis angle of 1.5° (see Figure 1 and Table 3). As visible from Figure 5, the bigger off-axis angle yields a ν_μ CC beam profile peaked around 1 GeV, which, because of the longer baseline, allows to be sensitive to the 1st minimum and the 2nd maximum of the neutrino oscillation. The previous configuration at 850 km was peaked around the 1st maximum.

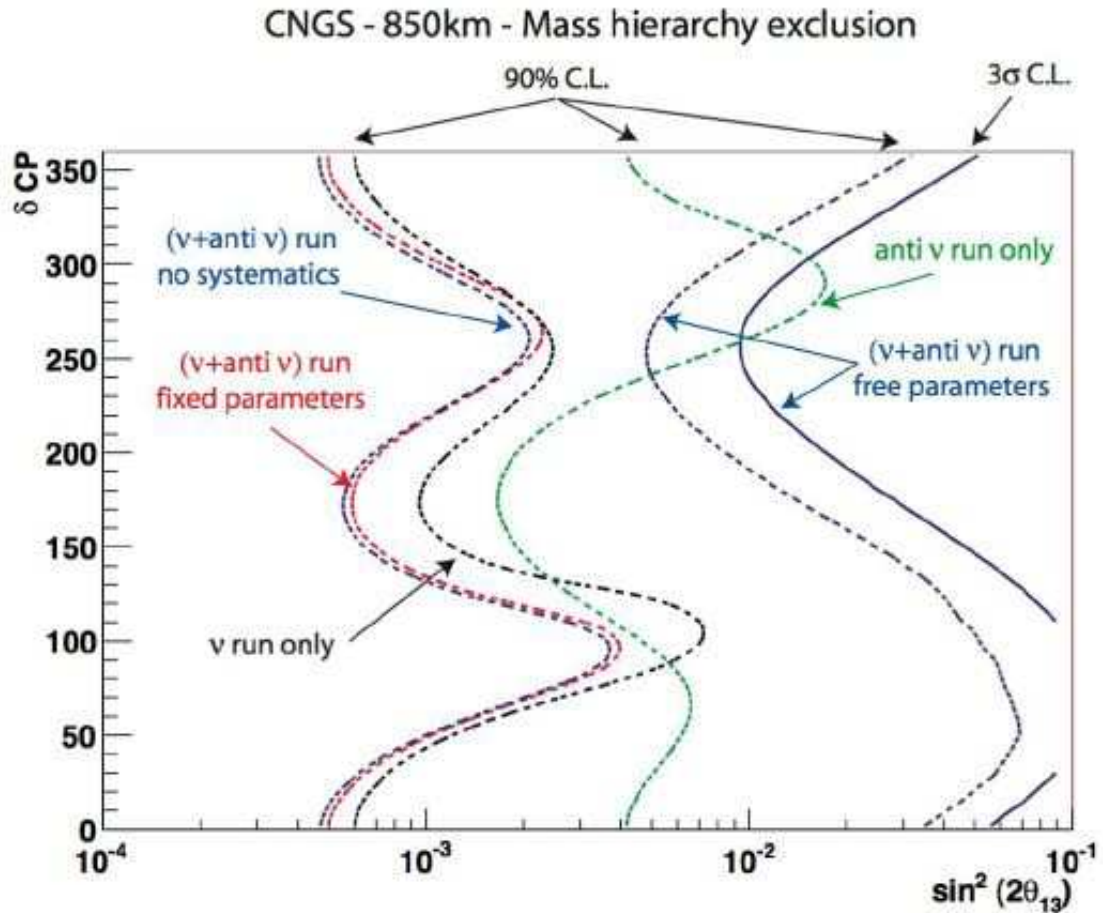


Figure 15: Sensitivity to exclude inverted mass hierarchy in the true $(\sin^2 2\theta_{13}, \delta_{CP})$ plane. The left-most dashed curve corresponds to neutrino and antineutrino polarity runs, with all oscillation parameters fixed and no systematic error at 90 %C.L. The corresponding curves for neutrino run only or antineutrino run only are also shown as dashed curves. The sensitivity leaving all other oscillation parameters free in the minimization is also shown as dashed curves. The corresponding sensitivity at 3σ is displayed as a continuous line.

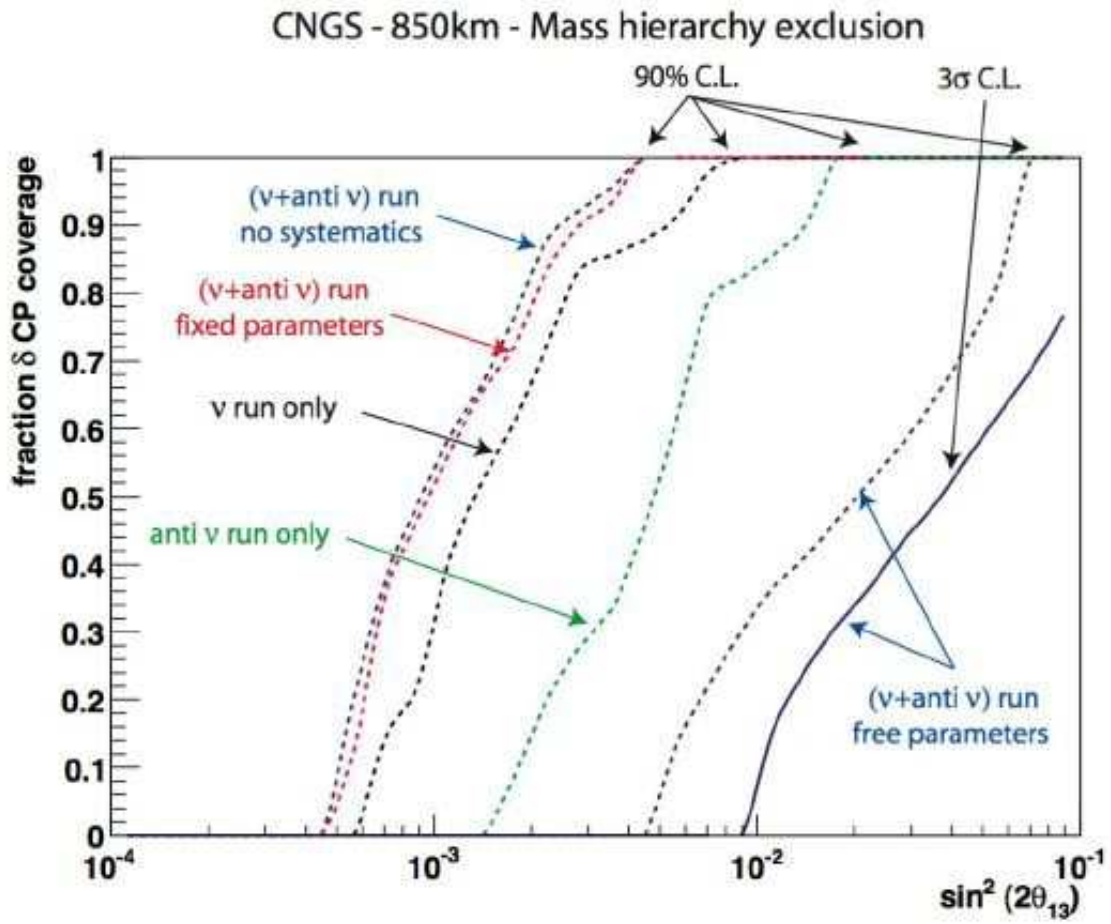


Figure 16: Sensitivity to discover exclude inverted mass hierarchy: the fraction of δ_{CP} coverage as a function of $\sin^2 2\theta_{13}$ corresponding to result plotted in Figure 15.

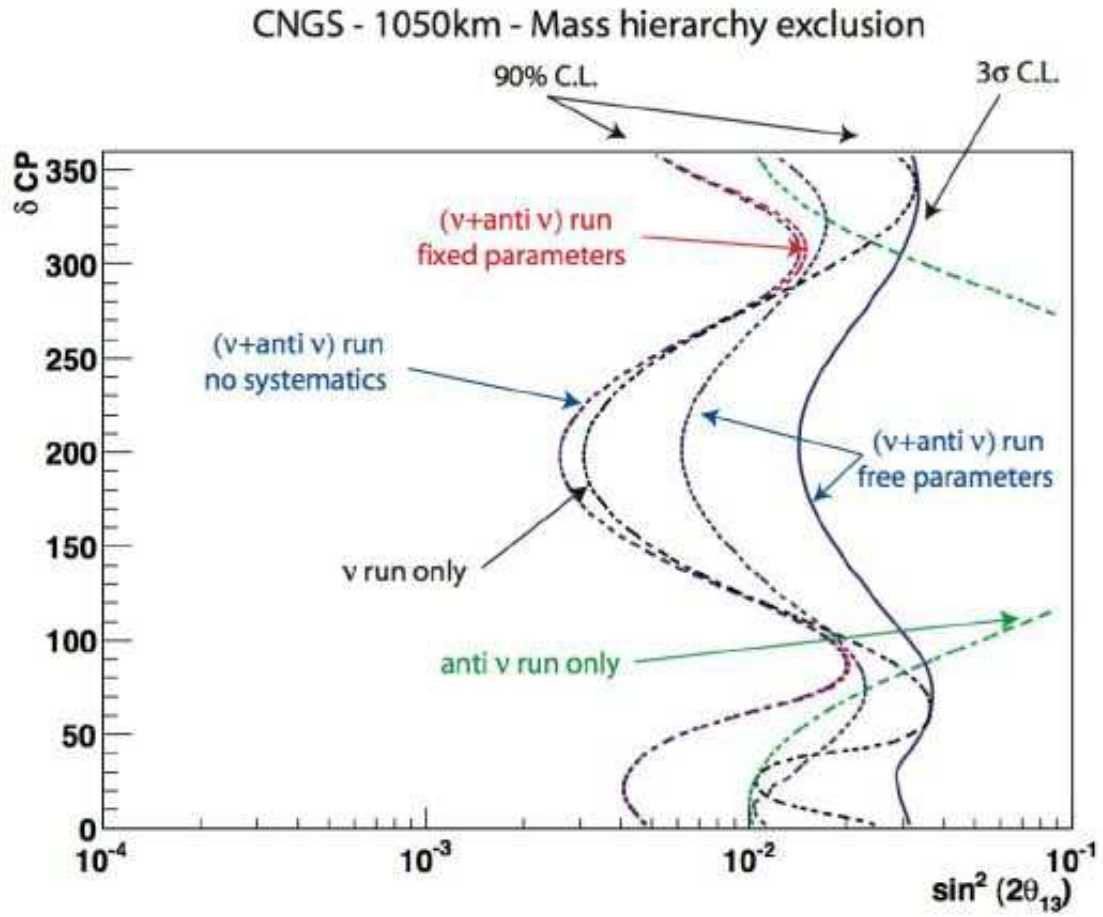


Figure 17: Same as Figure 15 for a baseline of 1050 km and OA1.5 configuration.

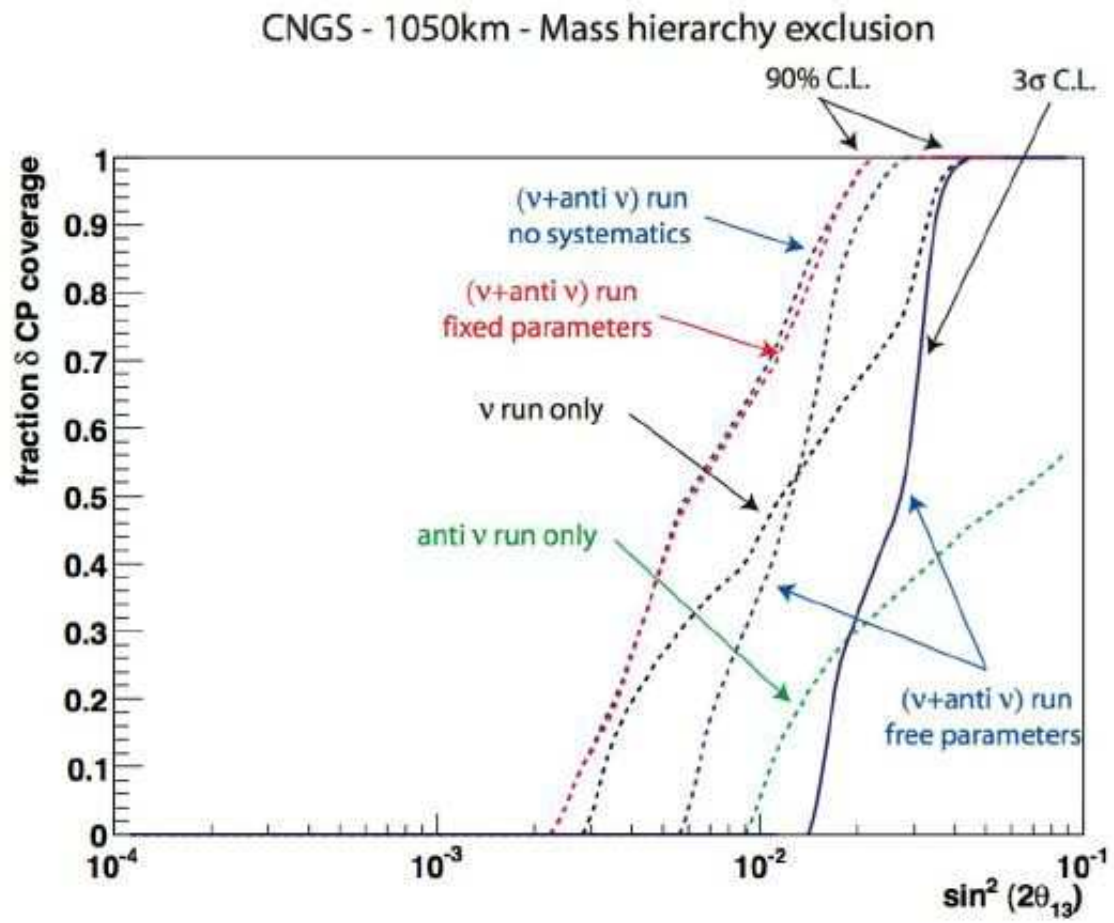


Figure 18: Same as Figure 16 for a baseline of 1050 km and OA1.5 configuration.

The results in the true $(\sin^2 2\theta_{13}, \delta_{\text{CP}})$ plane are reported in Figure 17. The left-most dashed curve corresponds to neutrino and antineutrino polarity runs, with all oscillation parameters fixed and no systematic error at 90 %C.L. The corresponding curves for neutrino run only or antineutrino run only are also shown as dashed curves. The sensitivity leaving all other oscillation parameters free in the minimization is also shown as dashed curves. The corresponding 3σ sensitivity (including correlations and degeneracy) is displayed as a continuous line.

The curves with fixed parameters have moved towards higher values of $\sin^2 2\theta_{13}$ given the decrease in statistics compared to the 850 km, OA0.75 case (effect of increased distance and off-axis angle). However, the sensitivity including parameter correlations and clone solution degeneracy has improved compared to the 850 km case. The dependence on δ_{CP} is also largely reduced. This confirms as expected that the energy region around the 1st minimum and 2nd maximum is important to resolve this issue.

This result can also be interpreted in terms of fraction of CP coverage, as shown in Figure 18. A coverage of 100% to determine the mass hierarchy can be reached for $\sin^2 2\theta_{13} \gtrsim 0.04$ at 3σ , while for the previous configuration at 850 km the full coverage could not be attained.

5.5 Sensitivity to mass hierarchy with two off-axis detectors

We have seen in the two previous sections that the configuration with a 100 kton detector at 850 km at an off-axis angle of 0.75° is optimal given the statistics to search for small values of θ_{13} , while a 100 kton detector at 1050 km at an off-axis angle of 1.5° is better for CP-violation and mass hierarchy determination.

In this section, we consider the splitting of the total mass of 100 kton into two similar detectors, one of 30 kton located at 850 km OA0.75, and a second of 70 kton located at 1050 km OA1.5. In this way, we expect a better coverage of the 1st maximum, 1st minimum and 2nd maximum of the neutrino oscillation probability, which should give the optimal condition for CP-violation and mass hierarchy determination.

The results in the true $(\sin^2 2\theta_{13}, \delta_{\text{CP}})$ plane are reported in Figure 19. The left-most dashed curve corresponds to neutrino and antineutrino polarity runs, with all oscillation parameters fixed and no systematic error at 90 %C.L. The corresponding curves for neutrino run only or antineutrino run only are also shown as dashed curves. The sensitivity leaving all other oscillation parameters free in the minimization is also shown as dashed curves. The corresponding 3σ sensitivity (including correlations and degeneracy) is displayed as a continuous line.

This result can also be interpreted in terms of fraction of CP coverage, as shown in Figure 20. A coverage of 100% to determine the mass hierarchy can be reached for $\sin^2 2\theta_{13} \gtrsim 0.02$ at 3σ , which is better than single detector configurations at either 850 km or 1050 km.

6 Comparison with the C2GT proposal

In Ref. [53], a deep-sea neutrino experiment with 1.5 Mt fiducial target mass in the Gulf of Taranto with the prime objective of measuring θ_{13} was discussed. The detector would also be exposed to the CERN neutrino beam to Gran Sasso in off-axis geometry. Monochromatic muon-neutrinos of ≈ 800 MeV energy are then the dominant beam component. Neutrinos are detected through quasi-elastic, charged-current reactions in sea water; electrons and muons are detected in a large-surface, ring-imaging Cherenkov detector. The profile of the seabed in the Gulf of Taranto allows for a moveable experiment at variable distances from CERN, starting at 1100

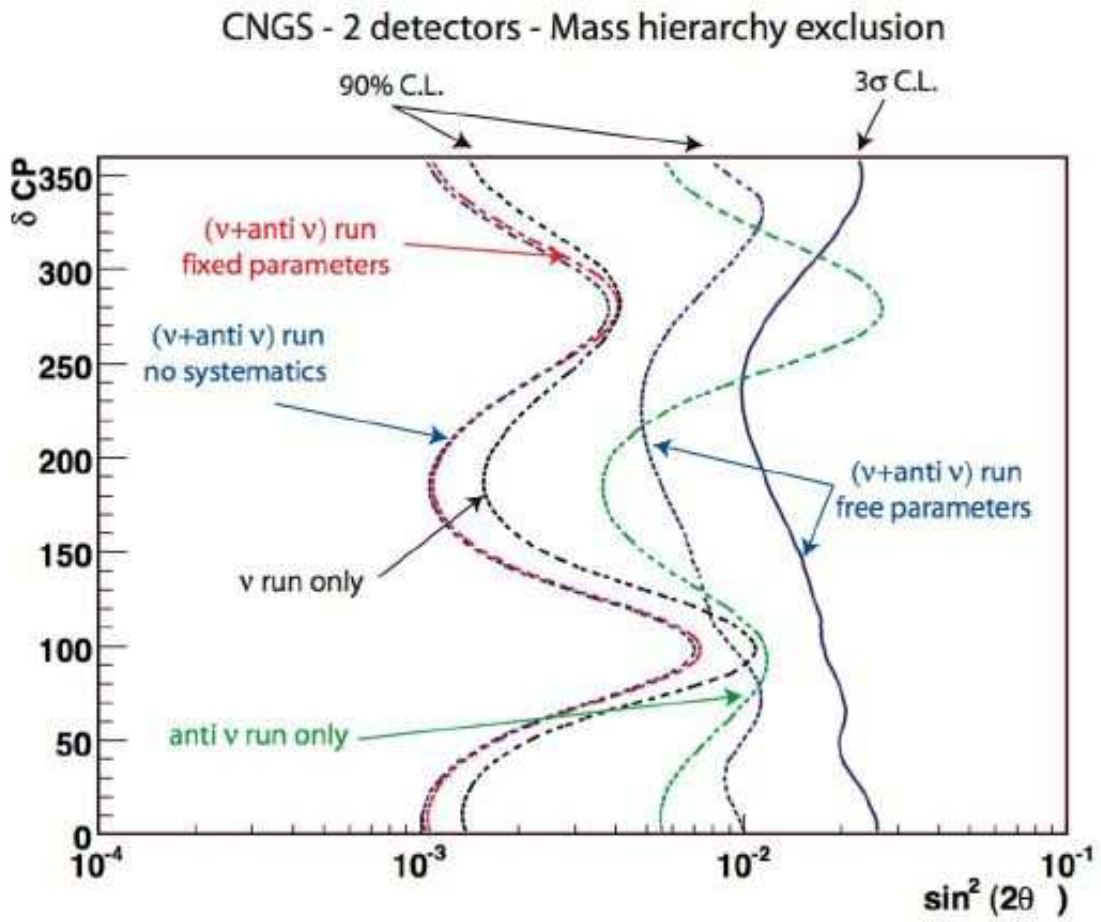


Figure 19: Same as Figure 15 for a two-detector configuration at baselines of 850 km OA0.75 and 1050 km OA1.5.

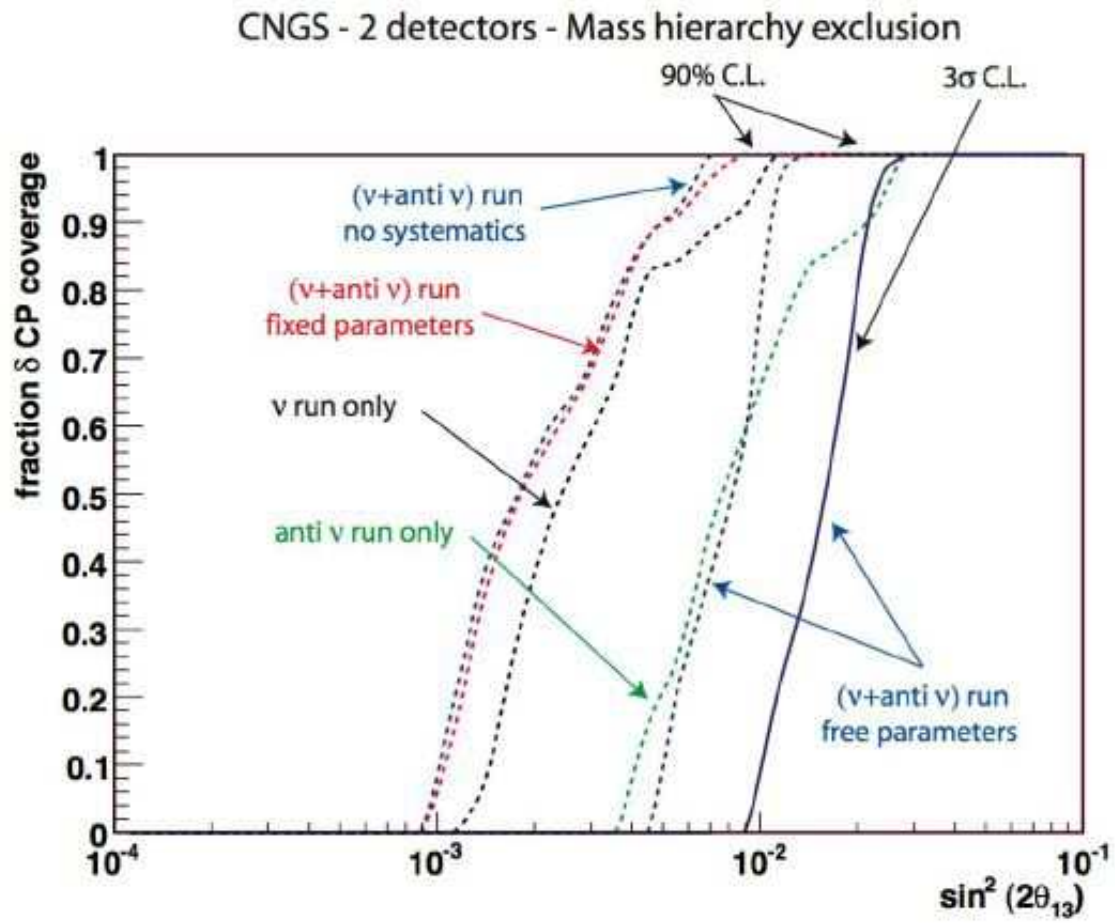


Figure 20: Same as Figure 19 with a two-detector configuration at baselines of 850 and 1050 km.

km. The appearance of electron-neutrinos will be observed with a sensitivity to $P(\nu_\mu \rightarrow \nu_e)$ as small as 0.0035 (90% CL) and $\sin^2 \theta_{13}$ as small as 0.0019 at 90% CL and for a CP phase angle $\delta_{\text{CP}} = 0^\circ$ and for normal neutrino mass hierarchy⁵.

The physics programme presented in this document differs from the C2GT proposal on the following points: (1) it concentrates on a smaller detector (100 kton instead of 1.5 Mt) on land rather than deep undersea, and (2) compensates the mass by an increased rate in neutrino flux. Our solution appears to us as a more attractive one. In addition, the use of the liquid Argon TPC instead of the deep sea water will provide better neutrino energy reconstruction and improved background suppression. Overall, the sensitivities shown in this document are superior to those of C2GT.

7 Comparison with other long baseline proposals

7.1 The T2KK proposal

In Ref. [54], the possibility of simultaneous determination of neutrino mass hierarchy and the CP violating phase by using two identical detectors placed at different baseline distances was explored. The focus was on a possible experimental setup using the JPARC neutrino beam assuming a beam power of 4MW and megaton (Mton)-class water Cherenkov detectors, one placed in Kamioka and the other somewhere in Korea. Under reasonable assumptions of systematic uncertainties, it was demonstrated that the two-detector complex with each fiducial volume of 0.27 Mton has potential of resolving neutrino mass hierarchy up to $\sin^2 2\theta_{13} > 0.03$ (0.055) at 2σ (3σ) CL for any values of δ_{CP} and at the same time has the sensitivity to CP violation by $4 + 4$ years running of ν_e and $\bar{\nu}_e$ appearance measurement. The authors interpreted the significantly enhanced sensitivity due to clean detection of modulation of neutrino energy spectrum, which was enabled by cancellation of systematic uncertainties between two identical detectors which would receive the neutrino beam with the same energy spectrum in the absence of oscillations.

The two-detector configuration considered in this document and described in Section 5.5 reaches very similar sensitivities to the T2KK one, and actually is slightly better in terms of CP-coverage. The CNGS programme discussed in this document is therefore very competitive with the configuration of two half-megaton Water Cherenkov detectors located in Japan and Korea.

Preliminary sensitivities of the T2K beam with 4 MW power coupled to potential large liquid Argon TPC detectors at Kamioka and/or in Korea have been recently presented [55]. More detailed studies are in progress to include the effects of oscillation parameter correlation and clone solution degeneracy. It is expected that a large liquid Argon TPC detector in Korea will provide a very competitive physics programme.

7.2 The FNAL-DUSEL proposal

In Ref. [56] the principal physics reasons for an experimental program in neutrino physics and proton decay based on construction of a series of massive water Cherenkov detectors located deep underground (4850 ft) in the Homestake Mine of the South Dakota Science and Technology Authority (SDSTA) was presented. The expected event rates and physics sensitivities for beams from both FNAL (1300 km distant from Homestake) and BNL (2540 km distant from Homestake) were discussed.

⁵Note that $\sin^2 2\theta_{13} \approx 4 \sin^2 \theta_{13}$ for small angles.

The configuration of a wide band super neutrino beam as in the case from FNAL or BNL coupled to the very long baselines to Homestake (1300 km from FNAL and 2540 km from BNL) offers optimal conditions to study the physics of $\sin^2 2\theta_{13}$, CP-violation and mass hierarchy [52].

Compared to configuration discussed in this document at the CNGS, the FNAL (or BNL) to Homestake proposal has similar sensitivity to $\sin^2 2\theta_{13}$, a slightly better CP-violation discovery reach (due to mass hierarchy degeneracy) and a better mass hierarchy determination owing to the longer baseline (> 1000 km). This advantage to FNAL-DUSEL can however be partially resolved by our 2 detector configuration at 850 km and 1050 km.

Overall, our calculations confirm the results of the authors of Ref. [52], which indicate that “wide band“ neutrino superbeams⁶ coupled to baselines in the 1000 km range offer very high physics potentials for $\sin^2 2\theta_{13}$ measurement, CP-violation discovery and mass hierarchy determination.

8 Synergies with betabeams or neutrino factories

The intrinsic limitations of conventional neutrino beams like the one discussed in this document, are overcome if the neutrino parents can be fully selected, collimated and accelerated to a given energy. This can be attempted within the muon or a beta decaying ion lifetimes. The neutrino beams from their decays would then be pure and perfectly predictable. The first approach brings to the Neutrino Factories [57], the second to the BetaBeams [58]. However, the technical and financial difficulties associated with developing and building these novel conception neutrino beams suggest for the middle term option to improve the conventional beams by new high intensity proton machines, optimizing the beams for the $\nu_\mu \rightarrow \nu_e$ oscillation searches and possibly CP-violating and matter effects, as is proposed in this document.

The 100 kton class far neutrino detectors coupled to the presently described upgraded CNGS could serve in a second phase as targets for an eventual BetaBeam or Neutrino Factory⁷, eventually complementing the series of measurements performed at the presently considered CNGS+ superbeam.

9 Outlook

This document discusses the physics opportunities of an upgraded CNGS program (CNGS+). It is based on the possible upgrade of the CERN PS or on a new machine (PS+) to deliver protons around 50 GeV/c with a power of 200 kW. Post acceleration to SPS energies followed by extraction to the CNGS target region should allow to reach MW power. The following issues will need to be addressed more carefully:

- The PS+ and SPS complex in order to transfer, accelerate and extract protons to reach MW power on the CNGS target region;
- The new high intensity CNGS target optics;
- The accessibility and modification capabilities of the CNGS targetry after 5 years of CNGS phase-1 operation.

⁶In our mind the term “wide band“ should merely indicate that the 1st maximum, 1st minimum and 2nd maximum of the neutrino oscillation are covered. It is not really necessary to cover too much of a large energy range above the 1st maximum and below the 2nd maximum.

⁷The use at a Neutrino Factory would however require a detector with magnetic field.

We propose that in the optimization of CERN accelerator complex the possibility of an upgraded CNGS program be considered. If good prospects for increased CNGS intensity were verified, more detailed studies for an off-axis detector location, away from the LNGS laboratory, presumably in a green-field at shallow depth [17], should be further investigated.

We think that the scientific programme addressed in this document could be part of a graded strategy to build next generation large detectors to explore θ_{13} and δ_{CP} -phase physics, to be eventually completed by more challenging new neutrino beams like beta-beams or neutrino factories if the outcome of the campaign of measurements at the presently discussed superbeam would (a) indicate their necessity (b) help guide in their optimization.

Acknowledgements

We acknowledge R. Garoby for useful discussions and for critical remarks. We thank T. Kajita and H. Minakata for useful discussions on long baseline neutrino oscillation experiments. We acknowledge F. Pietropaolo for providing us with the source of his CNGS fast simulation program. We thank the authors of GLOBES for freely distributing their code.

References

- [1] G. Acquistapace et al., “The CERN neutrino beam to Gran Sasso (NGS)”, Conceptual Technical Design, CERN 98-02 and INFN/AE-98/05 (1998). R. Baldy, et al. “The CERN neutrino beam to Gran Sasso (NGS)”, Addendum to report CERN 98-02, INFN/AE-98/05, CERN SL-99-034 DI and INFN/AE-99/05 (1999).
- [2] K. Kodama *et al.* [OPERA Collaboration], “OPERA: a long baseline ν_τ appearance experiment in the CNGS beam from CERN to Gran Sasso”, CERN/SPSC 99-20 SPSC/M635 LNGS-LOI 19/99.
- [3] G. DeLellis, Invited talk at the 8th international workshop on Neutrino Factories, Superbeams and Betabeams NUFAC06, August 2006, Irvine (USA).
- [4] T. Kajita, “Recent results from atmospheric and solar neutrino experiments,” Nucl. Phys. Proc. Suppl. **155**, 155 (2006).
- [5] Q. R. Ahmad *et al.* [SNO Collaboration], “Direct evidence for neutrino flavor transformation from neutral-current interactions in the Sudbury Neutrino Observatory,” Phys. Rev. Lett. **89**, 011301 (2002) [arXiv:nucl-ex/0204008].
- [6] K. Eguchi *et al.* [KamLAND Collaboration], “First results from KamLAND: Evidence for reactor anti-neutrino disappearance,” Phys. Rev. Lett. **90**, 021802 (2003) [arXiv:hep-ex/0212021].
- [7] B. Pontecorvo, *J. Expt. Theor. Phys.* **33**, 549 (1957) [Sov. Phys. JETP **6**, 429 (1958)]; B. Pontecorvo, *J. Expt. Theor. Phys.* **34**, 247 (1958) [Sov. Phys. JETP **7**, 172 (1958)]; Z. Maki, M. Nakagawa and S. Sakata, “Remarks On The Unified Model Of Elementary Particles,” *Prog. Theor. Phys.* **28** (1962) 870; B. Pontecorvo, *J. Expt. Theor. Phys* **53** (1967) 1717; V. Gribov and B. Pontecorvo, Phys. Lett. B **28**, 493 (1969).
- [8] M. Apollonio *et al.* [CHOOZ Collaboration], Phys. Lett. B **466**, 415 (1999) [arXiv:hep-ex/9907037].

- [9] C. Rubbia, “The Liquid Argon Time projection Chamber: a new concept for Neutrino Detector”, CERN-EP/77-08 (1977).
- [10] S. Amerio *et al.*, ”Design, construction and tests of the ICARUS T600 detector”, Nucl. Instrum. Meth. A 527 (2004) 329 and references therein.
- [11] P. Benetti *et al.*, “A 3 ton Liquid Argon Time Projection Chamber”, Nucl. Instrum. Meth. A 332 (1993) 395.
- [12] P. Cennini *et al.*, “Performance of a 3 ton Liquid Argon Time Projection Chamber”, Nucl. Instrum. Meth. A 345 (1994) 230.
- [13] F. Arneodo *et al.*, “The ICARUS 50 l LAr TPC in the CERN neutrino beam”, arXiv:hep-ex/9812006.
- [14] Y. Itow *et al.*, “The JHF-Kamioka neutrino project,” arXiv:hep-ex/0106019.
- [15] D. S. Ayres *et al.* [NOvA Collaboration], “NOvA proposal to build a 30-kiloton off-axis detector to study neutrino oscillations in the Fermilab NuMI beamline,” arXiv:hep-ex/0503053.
- [16] F. Ardellier *et al.*, “Letter of intent for double-CHOOZ: A search for the mixing angle $\theta(13)$,” arXiv:hep-ex/0405032.
- [17] A. Rubbia, Invited talk at the 8th international workshop on Neutrino Factories, Superbeams and Betabeams Nufact06, August 2006, Irvine (USA).
- [18] M. Furusaka *et al.* [Joint Project team of JAERI and KEK Collaboration], “The Joint Project for high-intensity proton accelerators,” KEK-REPORT-99-4
- [19] T. Ishida, Invited talk at 6th International workshop on Neutrino Beams and Instrumentation, CERN, September 4-9, 2006.
- [20] A. Marchionni, Talk at *Workshop on Long Baseline Neutrino Experiments*, Fermilab, March 6-7, 2006. http://www.fnal.gov/directorate/DirReviews/Neutrino_Wrkshp.html
- [21] R. Alber, *et al.*, Proton Driver Study Group FNAL-TM-2136, FNAL-TM-2169. <http://www-bd.fnal.gov/pdriver/>
- [22] J. Alessi *et al.*, AGS Super Neutrino Beam Facility, Accelerator and Target System Design, BNL-71228-2003-IR. April 15, 2003. <http://nwg.phy.bnl.gov/>
- [23] D. Mcginnis, Beams Document 1782-v7, FNAL, 2005.
- [24] CERN PAF working group.
- [25] R. Garoby, private communication.
- [26] R. Raja, Plenary talk at the 8th international workshop on Neutrino Factories, Superbeams and Betabeams Nufact06, August 2006, Irvine (USA).
- [27] D. Schmitz, Plenary talk at the 8th international workshop on Neutrino Factories, Superbeams and Betabeams Nufact06, August 2006, Irvine (USA).
- [28] P. Astier *et al.* [NOMAD Collaboration], “Prediction of neutrino fluxes in the NOMAD experiment,” Nucl. Instrum. Meth. A **515**, 800 (2003) [arXiv:hep-ex/0306022].

- [29] A. Rubbia, “Experiments for CP-violation: A giant liquid argon scintillation, Cerenkov and charge imaging experiment?,” arXiv:hep-ph/0402110.
- [30] D. B. Cline, F. Raffaelli and F. Sergiampietri, arXiv:astro-ph/0604548; D. B. Cline, F. Sergiampietri, J. G. Learned and K. McDonald, Nucl. Instrum. Meth. A **503**, 136 (2003) [arXiv:astro-ph/0105442].
- [31] L. Bartoszek *et al.*, “FLARE: Fermilab liquid argon experiments,” arXiv:hep-ex/0408121.
- [32] A. Ereditato and A. Rubbia, “Ideas for a next generation liquid Argon TPC detector for neutrino physics and nucleon decay searches”, Memorandum submitted to the CERN SPSC, April 2004.
- [33] A. Ereditato and A. Rubbia, “Conceptual design of a scalable multi-kton superconducting magnetized liquid argon TPC,” Nucl. Phys. Proc. Suppl. **155**, 233 (2006) [arXiv:hep-ph/0510131].
- [34] A. Badertscher, M. Laffranchi, A. Meregaglia, A. Muller and A. Rubbia, “First results from a liquid argon time projection chamber in a magnetic field,” Nucl. Instrum. Meth. A **555**, 294 (2005) [arXiv:physics/0505151].
- [35] A. Badertscher, M. Laffranchi, A. Meregaglia and A. Rubbia, “First operation of a liquid argon TPC embedded in a magnetic field,” New J. Phys. **7**, 63 (2005) [arXiv:physics/0412080].
- [36] A. Ereditato and A. Rubbia, “The liquid argon TPC: A powerful detector for future neutrino experiments and proton decay searches,” Nucl. Phys. Proc. Suppl. **154**, 163 (2006) [arXiv:hep-ph/0509022].
- [37] E. Kearns *et al.*, “A Proposal for a Detector 2 km Away From the T2K Neutrino Source”, document submitted to DOE NuSAG, May 2005.
- [38] A. Rubbia, Talk given at the ISS meeting held on July 3rd, 2006.
- [39] A. Rubbia and P. Sala, “A low-energy optimization of the CERN-NGS neutrino beam for a Theta(13) driven neutrino oscillation search,” JHEP **0209** (2002) 004 [arXiv:hep-ph/0207084].
- [40] E889 Collaboration, “Long Baseline Neutrino Oscillation Experiment”, Physics Design Report, BNL no 52455 (1995).
- [41] F. Pietropaolo, private communication.
- [42] M. Bonesini, A. Marchionni, F. Pietropaolo and T. Tabarelli de Fatis, “On particle production for high energy neutrino beams,” Eur. Phys. J. C **20**, 13 (2001) [arXiv:hep-ph/0101163].
- [43] M. Freund, “Analytic approximations for three neutrino oscillation parameters and probabilities in matter,” Phys. Rev. D **64**, 053003 (2001) [arXiv:hep-ph/0103300].
- [44] A. Cervera, A. Donini, M. B. Gavela, J. J. Gomez Cadenas, P. Hernandez, O. Mena and S. Rigolin, “Golden measurements at a neutrino factory,” Nucl. Phys. B **579**, 17 (2000) [Erratum-ibid. B **593**, 731 (2001)] [arXiv:hep-ph/0002108].

- [45] J. Burguet-Castell, M. B. Gavela, J. J. Gomez-Cadenas, P. Hernandez and O. Mena, Nucl. Phys. B **608**, 301 (2001) [arXiv:hep-ph/0103258].
- [46] H. Minakata and H. Nunokawa, “Exploring neutrino mixing with low energy superbeams,” JHEP **0110**, 001 (2001) [arXiv:hep-ph/0108085].
- [47] V. Barger, D. Marfatia and K. Whisnant, “Breaking eight-fold degeneracies in neutrino CP violation, mixing, and mass hierarchy,” Phys. Rev. D **65**, 073023 (2002) [arXiv:hep-ph/0112119].
- [48] P. Huber, M. Lindner and W. Winter, “Simulation of long-baseline neutrino oscillation experiments with GLOBES,” Comput. Phys. Commun. **167**, 195 (2005) [arXiv:hep-ph/0407333].
- [49] P. Huber, M. Lindner and W. Winter, “Superbeams versus neutrino factories,” Nucl. Phys. B **645**, 3 (2002) [arXiv:hep-ph/0204352].
- [50] R. J. Geller and T. Hara, “Geophysical aspects of very long baseline neutrino experiments,” Nucl. Instrum. Meth. A **503**, 187 (2001) [arXiv:hep-ph/0111342].
- [51] T. Ohlsson and W. Winter, “The role of matter density uncertainties in the analysis of future neutrino factory experiments,” Phys. Rev. D **68** (2003) 073007 [arXiv:hep-ph/0307178].
- [52] V. Barger, M. Dierckxsens, M. Diwan, P. Huber, C. Lewis, D. Marfatia and B. Viren, “Precision physics with a wide band super neutrino beam,” arXiv:hep-ph/0607177.
- [53] A. E. Ball *et al.*, “C2GT: Intercepting CERN neutrinos to Gran Sasso in the Gulf of Taranto to measure Theta(13),” CERN-PH-EP-2006-002
- [54] M. Ishitsuka, T. Kajita, H. Minakata and H. Nunokawa, “Resolving neutrino mass hierarchy and CP degeneracy by two identical detectors with different baselines,” Phys. Rev. D **72**, 033003 (2005) [arXiv:hep-ph/0504026].
- [55] A. Rubbia, Invited talk the 2nd International Workshop on a Far Detector in Korea for the J-PARC Neutrino Beam, July 2006, Seoul (Korea)
- [56] M. Diwan *et al.*, “Proposal for an experimental program in neutrino physics and proton decay in the homestake laboratory,” arXiv:hep-ex/0608023.
- [57] S. Geer, “Neutrino beams from muon storage rings: Characteristics and physics potential,” Phys. Rev. D **57** (1998) 6989 [Erratum-ibid. D **59** (1999) 039903], [hep-ph/9712290].
- [58] P. Zucchelli, “A novel concept for a anti- ν/e / ν/e neutrino factory: The beta beam,” Phys. Lett. B **532** (2002) 166.